Biomass Conversion and Biorefinery (2023) 13:1723–1750
https://doi.org/10.1007/s13399-020-01193-z

ORIGINAL ARTICLE

Utilization of factorial design methodology to optimize *Pr Red Hegxl* dye uptake and prediction of removal efficiency via artificial neural network: comparison of linear vs non-linear sorption isotherm and kinetic parameters

Alper Yargic[1] · Adife Seyda Yargic[2] · Nurgul Ozbay[2]

Received: 29 September 2020 / Revised: 26 November 2020 / Accepted: 1 December 2020 / Published online: 6 January 2021

Abstract

The evacuation of highly colored effluents in the ecosystem by textile industries generates extreme depredation to the environment and all living creatures. Sorption is preferred because of the wideness of biomass, and cost-efficient, minimized sludge in proportion to conventional treatment methods. A factorial experimental design and ANOVA techniques were utilized to examine the sorption of reactive Pr Red Hegxl dye by *Daphne* seed–based sorbents, and to optimize the operating conditions. The effects of main variables and their interaction effects on dye removal efficiency (%) were determined; pH was designated as significant at 95% confidence level for all types of sorbents. The maximum removal efficiencies (%) of *Daphne* seed and char were obtained as 70.8% and 83.2% when pH = 2, sorbent dosage = 0.4 g/50 mL, initial concentration = 50 mg/L, and temperature = 40 °C, respectively. 90.2% and 85.4% removal efficiencies were also attained for KOH- and K_2CO_3-activated carbons, respectively. Besides, artificial neural network models based on several back-propagation training algorithms and transfer functions were used to predict removal efficiency (%). The findings demonstrated that the proposed models had reasonable capabilities of predicting the removal efficiency (%). *Daphne* seed and carbonaceous products could be effectively used for the dye removal from aqueous solutions as affordable and abundant sorbent materials.

Keywords Artificial neural network · *Daphne* seed · Factorial design · Green carbon · Pr Red Hegxl · Sorption

1 Introduction

Dyes are presumed as one of the most hazardous pollutants among many classes of contaminants released into the environment. Most of the colored matters present in the surroundings and resistant to degradation by chemicals, water, light, and microbial operation are known as synthetic dyes [1]. Various industries such as textile, food, paper printing, dyeing, color photography, leather, and other industries have gradually used synthetic dyes [2, 3]. More than 100,000 different types of dyes are commercially available, and approximately 0.7 million tons of dyes are produced per annum [4–6]. Ten to 15% of the dyes are evacuated in effluents throughout the dyeing procedure [7]. Reactive dyes are highly soluble, and also have resistance to microbial attack and excellent fastness to the applied fabric; thus, these characteristics make them available in textile dyeing industries [3]. Colored and stable dyes have toxic and carcinogenic effects due to their chemical structures. Therefore, the release of dye effluents in receiving the body without treatment causes noxious problems [8]. The dyes are extremely apparent (esthetic pollution) and influence the marine life and food chain (chemical pollution) even in low concentrations [9]. Hence, many studies have concentrated on the removal of colored components from dye-containing wastewaters in recent years. Among various chemical and physical techniques such as coagulation, chemical oxidation, anaerobic treatment, and membrane filtration, sorption has developed into one of the essential procedures for decolorization of textile wastewaters. The reason is that other techniques are commonly ineffective in

✉ Adife Seyda Yargic
seyda.guler@bilecik.edu.tr

[1] Software Engineering Department, Engineering Faculty, Bilecik Seyh Edebali University, 11230 Bilecik, Turkey

[2] Chemical Engineering Department, Engineering Faculty, Bilecik Seyh Edebali University, 11230 Bilecik, Turkey

dye deduction, costly, and less compatible with a broad array of dye effluents. Several researchers have been studying different low-cost sorbents which comprise agricultural and industrial wastes, nanomaterials, carbonaceous materials, clay minerals, zeolites, biomass, and their adapted derivatives to enhance sorption capacity [10]. Some of these sorbents can be sequenced as coconut shell [10]; brown macroalga [11]; chitosan [12]; apple pulp/TiO_2 co-sorbent [13]; bifunctional chitin/lignin [14]; orange seeds [15]; *Lagerstroemia indica* seed [16]; polymer-clay nanocomposites [17]; mango leaf powder [18]; tomato waste [19]; multi-component biosorbent of pine, oak, hornbeam, and fir sawdust [20]; *Aspergillus niger* strain [21]; jujuba seeds [22]; *Panus tigrinus* [23]; wheat husk [24]; white pine [25]; Artocarpus odoratissimus leaves [26]; barbary fig skin [27, 28]; palm tree trunk lignin extract [29]; etc. Besides these abundant sorbents, nanomaterials such as gold, silica, carbon nanotube, metal oxide nanoparticles [30], graphene [31], and nanocomposites [32] are relatively expensive sorbents and used in sorption experiments. The dye removal efficiencies (%) of various biomass-based sorbents in the literature are given in Table 1.

A wild growing evergreen tree *Laurus nobilis L.* (*Bay*, *Sweet Bay*, *Bay Laurel*, or *Daphne*) is an insider of the *Lauraceae* subgroup (called *Apollo's Laurel* in mythology). The *Lauraceae* comprises 32 general and ~ 2000–2500 species. *Daphne* tree grows wild in the littoral zones of the Mediterranean and the Black Sea and is cultivated mostly in Europe and the USA as a decorative plant [47]. Italy, former Yugoslavia, and Turkey are among the most important producers of the botanical raw material. Grape-sized glossy purplish blackberries with three fragments of flesh, skin, and an inner kernel (single seed) bloom on *Daphne* trees [48]. *Daphne* is a plant of industrial importance and is utilized mainly for its leaf for spice and essential oil industry and its wood, generally used in foods, drugs, and cosmetics [49]. Laurel berries comprise both fixed and volatile oils consisting mainly of odorless lauric acid, myristic acid, and related compounds, which are mainly handled in soap production [50]. The aforementioned characteristics make the *Daphne* seed an attractive candidate for use as a potential source of renewable fuels and chemical feedstocks [51].

When a comprehensive literature search is carried out, it is seen that much work has been done on the discovery of new adsorbents for use in the removal of toxic substances. However, it is observed that the identification of low-cost adsorbents with high adsorption capacity is a research and development area. In our previous studies, the development of biomass-based and nanostructure-doped adsorbents for the removal of various dyes and heavy metals has been investigated. In this study, the effect of different activation agents

Table 1 Removal efficiency (%) values for various dye sorption processes in the literature

Adsorban	Adsorbate	Removal efficiency (%)	Ref.
The marine green alga Enteromorpha flexuosa	1) Crystal violet (CV) 2) Methylene blue (MB)	1) 90.3% 2) 93.4%	[33]
The Mediterranean seagrass *Posidonia oceanica* (L.) leaf sheaths	Reactive Red 228	80%	[34]
Shrimp shell	Acid Blue 25	95.64%	[35]
1) Raw Irvingia gabonenses (dika nut) (DN) 2) Its acid-treated form (ADN)	Rhodamine B	1) 78.69% 2) 97.05%	[36]
Sunflower seed husk (Helianthus annuus)	Methylene Blue	95%	[37]
Palm flower activated carbon	Amido Black 10B (AB10B)	95%	[38]
Sunflower seed shells	Orange 16	87.07%	[39]
Phoenix dactylifera seeds	Congo red	90.15%	[40]
Bengal Gram Seed Husk	Congo red	92%	[41]
1) Raw beetroot seeds (BS) 2) H_3PO_4 activated beetroot seeds (H_3PO_4-BS)	1) Methylene blue (MB) and malachite green (MG) 2) Methylene blue (MB) and malachite green (MG)	1) 86.1% and 90.5% 2) 98.7% and 96.6%	[42]
Date palm rachis (RPK)	Reactive dye (BEZAKTIV Red S-MAX)	94.37%	[43]
Pine Cone activated carbon	Congo Red	80.6%	[44]
Mango seed kernel powder	Methylene blue	96.17%	[45]
Aminated hulls of sunflower seeds	1) Reactive Black 5 2) Reactive Yellow 84 3) Acid Yellow 23 4) Acid Red 18	1) 84% 2) 92% 3) 85% 4) 81%	[46]
1) Daphne seed (DS) 2) Its char (DSC) 3) KOH-activated carbon (DSB) 4) K_2CO_3-activated carbon (DSS)	Pr Red Hegxl	1) 70.8% 2) 83.2% 3) 90.2% 4) 85.4%	This sudy

Table 2 Factors and their levels studied in full factorial design

Factors	Levels	
	1	2
pH (A)	2	8
Sorbent dosage, g/50 mL (B)	0.1	0.4
Temperature, °C (C)	20	40
Contact time, min (D)	60	120
Initial concentration, mg/L (E)	50	100

and carbonization on sorbent structure and dye removal efficiency were investigated. It is known that it is both expensive and time-consuming to examine each parameter that affects the sorption process individually. In this context, the use of experimental design methods helps to avoid these disadvantages.

Experimental design is a splendid method to investigate the main and interaction effects of all factors simultaneously. Formerly conducted researches have not yet emphasized the full factorial design of reactive dye uptake experimental terms via *Daphne* seed sorbent. Accordingly, the availability of *Daphne* seed as biosorbent, its char, K_2CO_3, and KOH-activated *Daphne* seed as adsorbents for Pr Red Hegxl dye removal from aqueous solutions was examined in this research. Turkey is an agricultural country and has diverse and abundant biomass resources. Besides, Turkey is one of the main producers and suppliers of *Daphne* trees, so it can focus on the evaluation of the wild-growing plant as a renewable fuel source and chemical feedstocks. Considering that this raw material is utilized as a fuel through thermochemical conversion methods, it is important to investigate its usage as an adsorbent. As a result, this study will be a model to evaluate the carbonaceous materials produced directly by carbonization as well as the by-product obtained after the pyrolysis process (char) as an adsorbent. Our literature survey showed that no experimental data were available regarding the dye removal efficiency of *Daphne* seeds and its carbonaceous derivatives, the optimization of sorption conditions, and the prediction of dye uptake%. In order to analyze the significance of five experimental factors (pH, sorbent dosage, initial dye concentration, temperature, and contact time) on the color uptake, 2^5 experimental design and statistical analyses were applied. Artificial neural network (ANN) methods are widely used in various research areas due to their ability to reliably and successfully determine both linear and nonlinear relationships between multiple input-output variables [52]. Therefore, the experimental data were also analyzed via ANN data modeling to predict the dye removal efficiency (%) of *Daphne* seed–based sorbents. Finally, linear and non-linear forms of Freundlich, Langmuir, Temkin, and Dubinin-Radushkevich equations were selected to perform the equilibrium data analysis, and three kinetic models (pseudo-first- and second-order, intraparticle diffusion) were focused on predicting the uptake of reactive dye. Non-linear regression was performed by using the Solver add-in function in Microsoft Excel (Microsoft

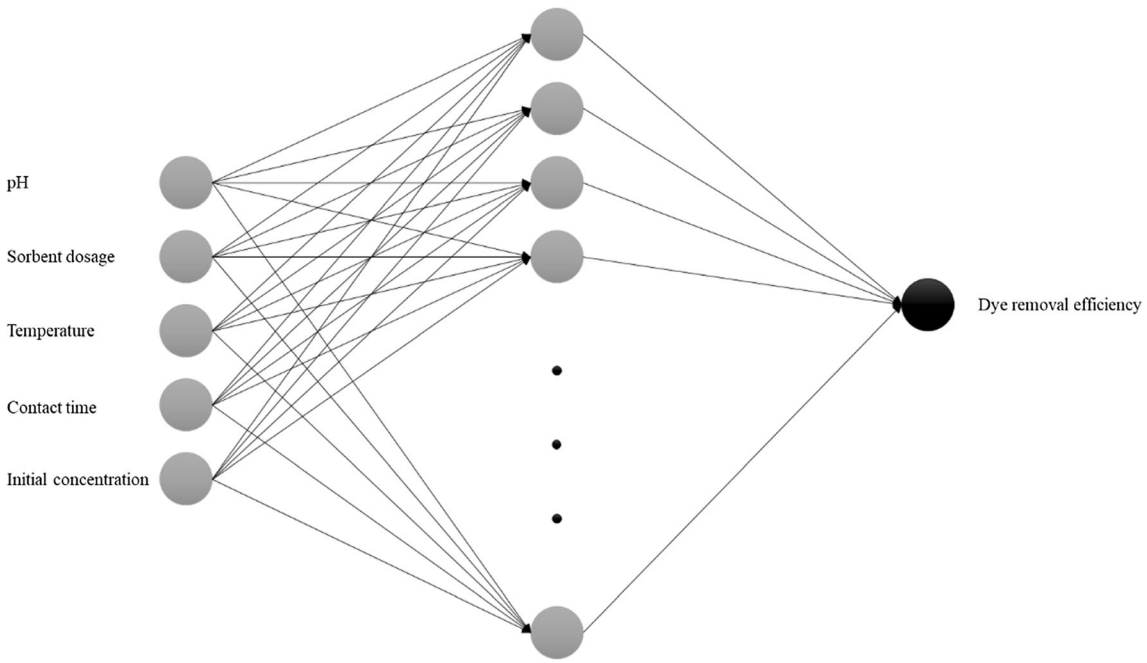

Fig. 1 Schematic diagram of the ANN model for dye removal efficiency (%)

Corporation). Two error functions (R^2 and RMSE) were applied to evaluate the isotherm and kinetic models.

2 Materials and methods

The sorbent type selection and application technique are fundamental for dye removal; hence, sorbent should be characterized in detail and designation of working settings should be done meticulously.

2.1 Sorbents and sorbates arrangement

Daphne seed (DS) attained from a soap factory in Hatay (Turkey) was air-dried, crushed, and sieved to obtain mean sizes. Carbonization temperature and heating rate were selected as 550 °C and 10 °C/min to propagate carbonaceous product (DSC). The raw material (100 g) was mixed with KOH or K_2CO_3 to get the saturation ratio of chemical agents to the precursor as 75 wt%. First, this mixture was mixed homogeneously for 24 h and then oven-dried at 85 °C for 24 h. The obtained material was subsequently carbonized at a heating rate of 10 °C/min until the activation temperature was succeeded at 700 °C. The samples were upheld for 60 min in the final activation temperature and then cooled down to room temperature. The carbonized materials were washed with distilled water to eliminate residual chemicals up to the pH value of the activated carbon was neutral. Washed samples were dried at 105 °C for 24 h to prepare the final activated carbons. Samples with an average particle size of 0.425 < Dp < 2 mm were kept in plastic flasks for further use, and they were utilized as sorbents. The sorbent nomenclature designated was as follows: DS = *Daphne* seed, DSC = *Daphne* seed char, DSB = *Daphne* seed base activation (KOH), and DSS = *Daphne* seed salt activation (K_2CO_3).

Reactive textile dye Pr Red Hegxl (RH, color index: 293755) was handled without any purification method. Distilled water was added in dye solutions to forestall and diminish possible impurities. Standard dye solution (1000 ppm) was confected by dispersing 1.0 g of RH dye in 1000 mL of distilled water. Several dye concentrations (50–100 mg/L) were prepared by subtilizing the stock dye solution. 0.1 M NaOH or 0.1 M HCl were supplemented to arrange the solution pH which was followed by a digital pH meter Thermo Scientific Orion 3 Star.

2.2 Sorbent characterization

Various characterization techniques were applied to identify sorbent properties. The carbon, hydrogen, nitrogen, and oxygen contents of sorbents were detected by an elemental analyzer (Leco CNH628 S628) with helium, dry air, and oxygen gases. The whole organic samples were combusted completely in the elemental analyzer's furnace at 950 °C. The proximate analysis of DS was involved in the structure and preliminary analyses. Moisture, ash, volatile matter, and fixed carbon contents of biosorbent were analyzed by ASTM E 871-82, ASTM D 1102-84, and ASTM E 872-82 and ASTM E 870-82 standard test methods, respectively. Functional groups were determined by applying the ATR technique (with a diamond protected attenuated total reflectance crystal unit) in Fourier transform infrared (FT-IR) spectroscopy (Perkin Elmer Spectrum 100). The FT-IR spectrums of sorbents were obtained in the range of 4000–400 cm^{-1} with a resolution of 4 cm^{-1} after 100 scans. BET surface analyzer (Micromeritics ASAP 2020) was utilized to determine the specific surface area and pore diameter of the sorbents.

Table 3 The results for ultimate and proximate analyses

Ultimate analysis of *DS* and *DSC*				
Component (%)	**DS**	**DSC**	**DSB**	**DSS**
C	44.54	87.27	77.17	80,24
N	0.81	3.59	1,12	1,31
H	7.96	5.12	6,37	5,23
O[a]	46.69	4.02	15,34	13,22
HHV (MJ/kg)	18.13	36.18	32.52	32.30
Proximate analysis of *DS*				
Preliminary analysis	wt%			
Moisture	7.52			
Ash	3.93			
Volatile	75.35			
Fixed carbon[a]	13.20			
Structural analysis	wt%			
Holocellulose	81.67			
Hemicellulose	24.49			
Extractive material	6.28			
Lignin	8.12			
Cellulose[a]	57.18			

[a] Estimated by difference

2.3 Batch sorption experiments

Batch sorption studies were accomplished to investigate the effect of parameters such as pH, sorbent dosage, initial dye concentration, temperature, and contact time on RH dye uptake. Tests were performed in a group of conical test tubes involving 50 mL dye solution of various experimental circumstances. The suspensions were then percolated, and dye quantity in the filtrate was determined. Calibration curves and concentration values were elaborated at λ_{max}, 533 nm for RH dye via the measurement of absorbance by a UV/visible

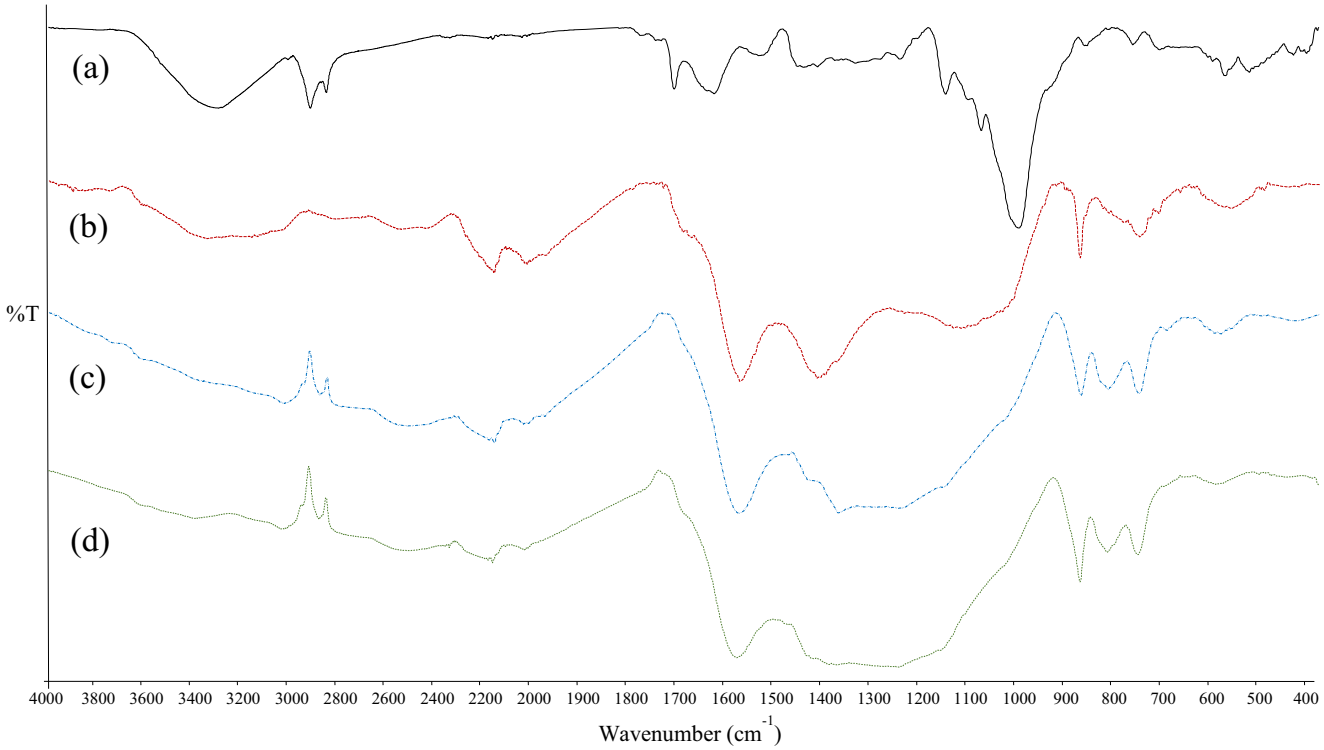

Fig. 2 FT-IR spectrums of **a** DS, **b** DSC, **c** DSB, and **d** DSS

spectrophotometer (Agilent Cary 60 UV-Visible Spectrophotometer).

The dye removal efficiency (η) and the sorption capacity of dye (q_e) from aqueous solutions were specified by Eqs. (1) and (2) [4]:

$$\eta = [(C_0 - C_e)/C_0]100 \quad (1)$$

$$q_e = (C_0 - C_e)V/W \quad (2)$$

where C_0 and C_e (mg/L) are dye concentrations in the liquid phase at initial and equilibrium, respectively. q_e is the amount of dye sorbed on the sorbent (mg/g), V (L) is the volume of the dye solution, and W (g) is the used sorbent amount.

2.4 Equilibrium modeling, kinetic, and thermodynamic studies

The sorption data can be examined handling familiar equilibrium isotherms to attain some insight into the sorption mechanism [53]. The mathematical correlation between the amount of adsorbate and equilibrium adsorbate concentration residual in the solution at a constant temperature is expressed by the sorption isotherms [54]. Linear and non-linear forms of Freundlich, Langmuir, Temkin, and Dubinin-Radushkevich isotherm models were utilized for analyzing the experimental data of RH dye and for examining the equilibrium characteristics of sorption.

The Freundlich isotherm is given in Eq. (3) and is a commonly applied empirical statement that computes for the surface heterogeneity, exponential distribution of sorbent's active sites, and their energies towards sorbate [55, 56]. In Eq. (4), the Langmuir isotherm assumes a homogeneous surface for the sorbent and equivalent sorption energies for each site, without lateral interaction and steric coaction between the sorbed molecules [57, 58]. Temkin isotherm, where the effects of extremely large and low concentration values on the surface interactions are ignored, assumes that the adsorption heat (H_{ads}) reduces linearly rather than logarithmically due to the rise in the adhesion of the molecules in the adsorbent-adsorbate layer (Eqs. (5) and (6)). Finally, equations of the Dubinin-Radushkevich adsorption isotherm model, in which the distribution of Gaussian energy on heterogeneous surfaces is used to define the adsorption mechanism, are given in Eqs. (7) and (8) [59].

Freundlich isotherm : (3)

$$Linear\ form : \log q_e = \log K_F + (1/n)\log C_e \quad (3.a)$$

$$Non\text{-}linear\ form : q_e = K_F C_e^{1/n} \quad (3.b)$$

Langmuir isotherm : (4)

$$Linear\ form : C_e/q_e = 1/(K_L q_m) + C_e/q_m \quad (4.a)$$

$$Non\text{-}linear\ form : q_e = (q_m K_L C_e)/(1 + K_L C_e) \quad (4.b)$$

Temkin isotherm : (5)

Table 4 Isotherm constants and regression correlation coefficients for sorption of *RH* dye

Models	Parameters	Sorbent type			
		DS	DSC	DSS	DSB
Langmuir					
Linear model	R^2	1.000	0.998	0.996	0.996
	q_m (mg/g)	19.23	58.82	28.57	33.33
	K_L (L/mg)	0.1534	0.0256	0.0443	0.0592
	RMSE	0.0196	0.0130	0.0465	0.0354
Non-linear model	R^2	0.999	0.999	0.995	0.994
	q_m (mg/g)	19.00	58.36	28.47	33.21
	K_L (L/mg)	0.1566	0.0255	0.0438	0.0583
	RMSE	0.0642	0.1599	0.4502	0.6192
Freundlich					
Linear model	R^2	0.954	0.996	0.996	0.995
	n	3.83	1.48	2.08	2.14
	K_F (mg/g(L/mg)$^{1/n}$	6.05	2.45	2.96	4.08
	RMSE	0.0237	0.0123	0.0099	0.0116
Non-linear model	R^2	0.951	0.998	0.997	0.996
	n	4.14	1.53	2.15	2.22
	K_F (mg/g(L/mg)$^{1/n}$	6.47	2.66	3.12	4.32
	RMSE	0.8924	0.5060	0.3509	0.4789
Temkin					
Linear model	R^2	0.980	0.988	0.995	0.995
	B	3.3867	11.8100	6.4805	7.4425
	b_t (J/mol)	768.38	220.35	401.56	349.65
	A_T (L/g)	2.8405	0.2888	0.3964	0.5462
	RMSE	0.4622	0.9335	0.3596	0.4548
Non-linear model	R^2	0.980	0.988	0.995	0.995
	B	3.3866	11.8097	6.4804	7.4425
	b_t (J/mol)	768.39	220.35	401.56	349.65
	A_T (L/g)	2.8407	0.2887	0.3964	0.5462
	RMSE	0.5660	1.1433	0.4405	0.5569
Dubinin-Radushkevich					
Linear model	R^2	0.957	0.896	0.892	0.885
	q_m (mg/g)	16.39	25.93	18.30	21.71
	β (mol^2/kJ^2)	3.7132	9.0646	10.0640	5.6681
	E (kJ/mol)	0.3669	0.2349	0.2229	0.2970
	RMSE	0.0536	0.1572	0.1242	0.1354
Non-linear model	R^2	0.934	0.858	0.842	0.827
	q_m (mg/g)	16.49	28.28	18.99	22.58
	β (mol^2/kJ^2)	3.8292	11.9729	11.5210	6.5348
	E (kJ/mol)	0.3614	0.2044	0.2083	0.2766
	RMSE	1.0330	3.9368	2.4800	3.2436

$$Linear\ form: q_e = BlnA_T + BlnC_e \quad (5.a)$$

$$Non{-}linear\ form: q_e = BlnA_T C_e \quad (5.b)$$

$$B = RT/b_t \quad (6)$$

Dubinin−Radushkevich isotherm : (7)

$$Linear\ \ form: \ln q_e = \ln q_m - \beta\varepsilon^2 \quad (7.a)$$

$$Non{-}linear\ \ form: q_e = q_m \exp(-\beta\varepsilon^2) \quad (7.b)$$

$$\varepsilon = RTln(1 + 1/C_e) \quad (8)$$

where C_e (mg/L) is the dye concentration of solution at equilibrium; q_e (mg/g) is the sorbed dye amount per unit weight of sorbent. Besides, K_L (L/mg) and q_m (mg/g) are Langmuir constants pertained to the rate of sorption and maximum sorption capacity, respectively. The heterogeneity factor and the Freundlich sorption constant are symbolized as n and K_F (mg/g(L/mg)$^{1/n}$), respectively. *1/n* value and K_F are pertinent to the sorption intensity and the bonding energy, respectively. The intercept (K_F) and the slope (*1/n*) are attained by drawing lnq_e curve in term of lnC_e. A_T is the Temkin isotherm equilibrium binding constant (L/g), B is the constant related to the heat of adsorption, b_t is the Temkin isotherm constant (J/mol), R is the universal gas constant (8.314 J/molK), and T is the absolute temperature (K). In Dubinin-Radushkevich equations, ε and β denote the Polanyi potential and the activity coefficient (mol^2/kJ^2), respectively. The mean sorption energy E (kJ/mol) is

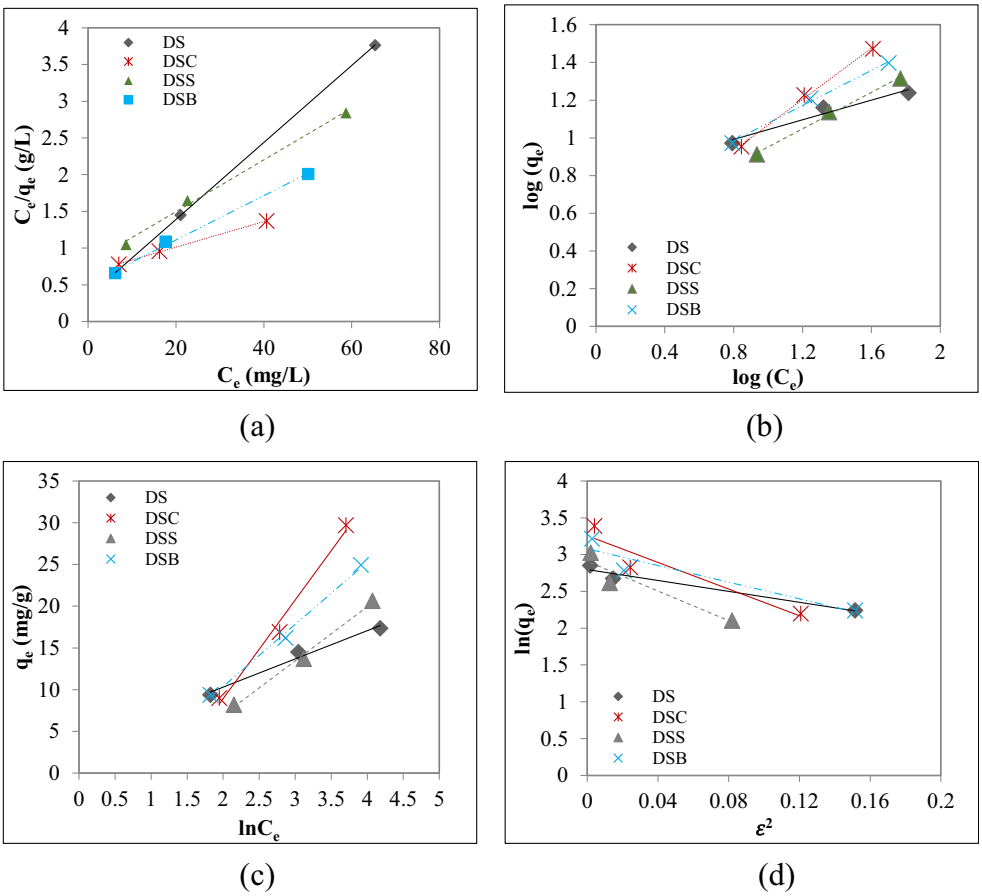

Fig. 3 Linear isotherm models for sorption of RH dye on DS and carbonaceous materials: **a** Langmuir, **b** Freundlich, **c** Temkin, and **d** Dubinin-Radushkevich

calculated from $1/\sqrt{2\beta}$ expression.

Kinetic studies are essential to define the equilibrium data for sorption. The potential mechanism of RH dye sorption process was estimated from pseudo-first-order (Eq. (9)), pseudo-second-order (Eq. (10)), and intraparticle diffusion (Eq. (11)) models by utilizing the experimental data of kinetic studies. According to the pseudo-first-order model, the proportion of alteration of solute capturing with time is immediately proportional to the variation in saturation concentration and the amount of solid retaining with time [60]. The rate-limiting step is the surface adsorption that comprises chemisorption in the pseudo-second-order model, where the removal from a solution is based on physicochemical interactions between the two phases [61]. The intraparticle diffusion model expresses that the sorption technique for a solute-solvent system involves the mass transfer of adsorbate (film diffusion), and surface diffusion. In this case, mass transfer by film diffusion takes place independently, while diffusion onto the sorbent surface may occur simultaneously [62].

Pseudo−first−order kinetics : (9)

$$\textit{Linear form} : \log\left(q_e - q_t\right) = \log q_e - (k_1 t)/2.303 \quad (9.a)$$

$$\textit{Non-linear form} : q_t = q_e\left(1 - e^{-k_1 t}\right) \quad (9.b)$$

Pseudo−second−order kinetics : (10)

$$\textit{Linear form} : t/q_t = 1/\left(k_2 q_e^2\right) + (1/q_e)t \quad (10.a)$$

$$\textit{Non-linear form} : q_t = \left(k_2 q_e^2 t\right)/(1 + k_2 q_e t) \quad (10.b)$$

Intraparticle diffusion model : $q_t = k_i t^{1/2} + C$ (11)

where t is the contact time (min), q_e and q_t (mg/g) are the amounts of RH dye sorbed at equilibrium and at time t (min), and k_1 and k_2 are the rate constants of pseudo-first-order sorption (min^{-1}) and of pseudo-second-order sorption (g/mg·min), respectively [13]. k_i is the intraparticle diffusion rate constant with C as intercept along q_t axis. The boundary layer thickness can be acquired from the C value; thus, a large intercept implies a great boundary layer effect [63].

The best-fitted isotherm or kinetic model was found by applying both linear and non-linear regression; besides, the correlation coefficients of R^2 and the root mean square error (RMSE) were calculated to crosscheck the applicability of model equations. The best fitted model chosen is the one of with highest R^2 and the lowest RMSE values. In general, non-linear regression gives a more convenient

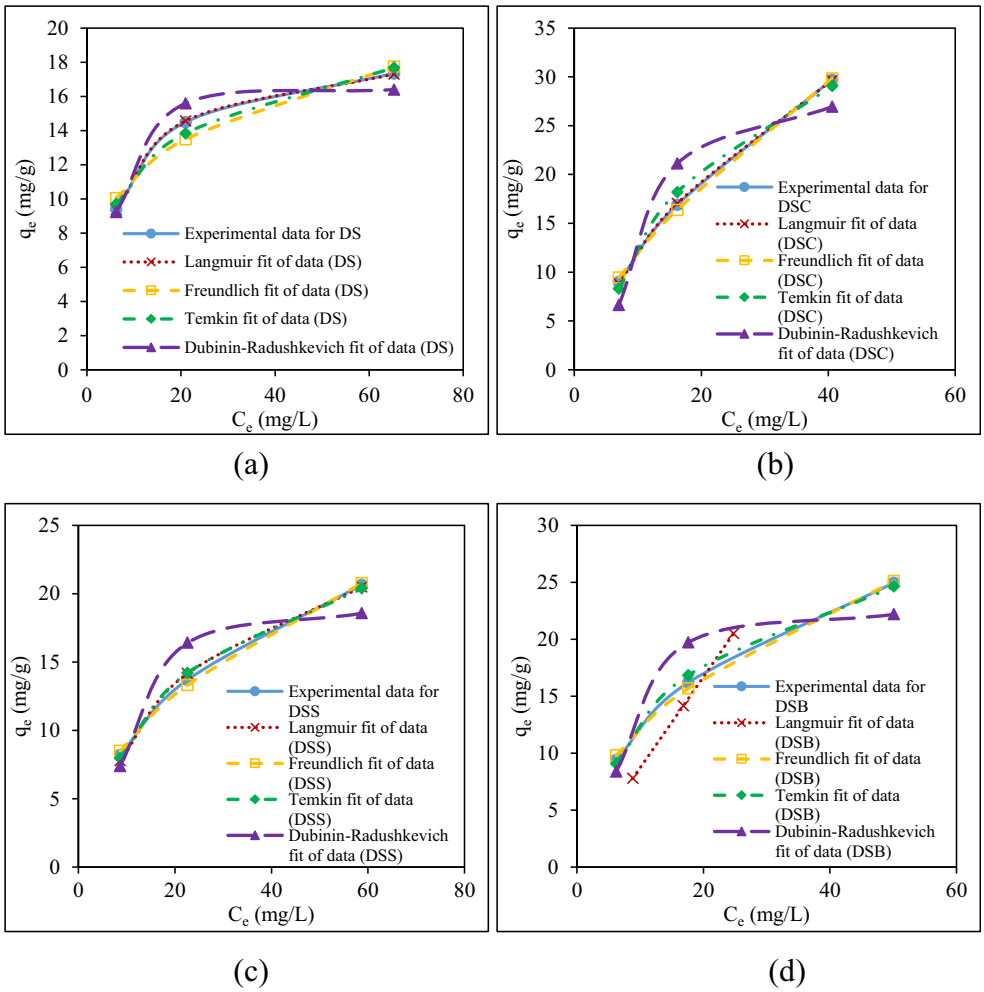

Fig. 4 Predicted curve fits for the sorption isotherms of RH dye on **a** DS, **b** DSC, **c** DSS, and **d** DSB obtained by non-linear approach at 40 °C

and certain determination of model parameters than the linear regression method [64]. The steps in the study of Hossain et al. [65] were followed in the performing of the non-linear regression process through the solver function. Finally, the residual plots were used to determine the adequacy of the regression models. The residual plot of the applied isotherm or kinetic model with a clean pattern demonstrates that the model is inadequate and the model errors are constant. In contrast, a uniform residual distribution proves the adequacy of the model [66].

To perform thermodynamic studies, the temperature effect on the sorption was analyzed through the experiments implemented at different temperatures (293, 303, and 313 K). The thermodynamic parameters associated with the adhesion process of the RH dye to *Daphne*-based sorbents were calculated using Eqs. (12–14). According to the Van't Hoff equation, it is known that the Gibbs free energy change (ΔG°) of the sorption process depends on the equilibrium constant. By applying Eq. (14), the entropy (ΔS°) and enthalpy (ΔH°) changes were specified from the intercept and slope of the lnK_D versus $1/T$ plot, respectively.

$$\Delta G^{\circ} = -RTlnK_D \tag{12}$$

$$\Delta G^{\circ} = \Delta H^{\circ} - T\Delta S^{\circ} \tag{13}$$

$$lnK_D = \left(\Delta S^{\circ}/R\right) - \left(\Delta H^{\circ}/RT\right) \tag{14}$$

where K_D is the equilibrium constant (L/g), R is the universal gas constant (8.314 J/mol K), and T is the absolute temperature (K) [19, 67].

2.5 Modeling by full factorial design

The total count of experiments, time, and whole research cost were reduced by applying factorial design; thus, the best overall optimization of the process is succeeded [68–70]. Factorial design involves better accuracy in forecasting the effects of the entire main factor and interactions of different factors. Two-level factorial design is one of the easiest forms of factorial designs. All combinations of the experimental factor levels are studied to obtain responses in a full factorial experiment [69]. A 2^5 full factorial design including 32 experiments

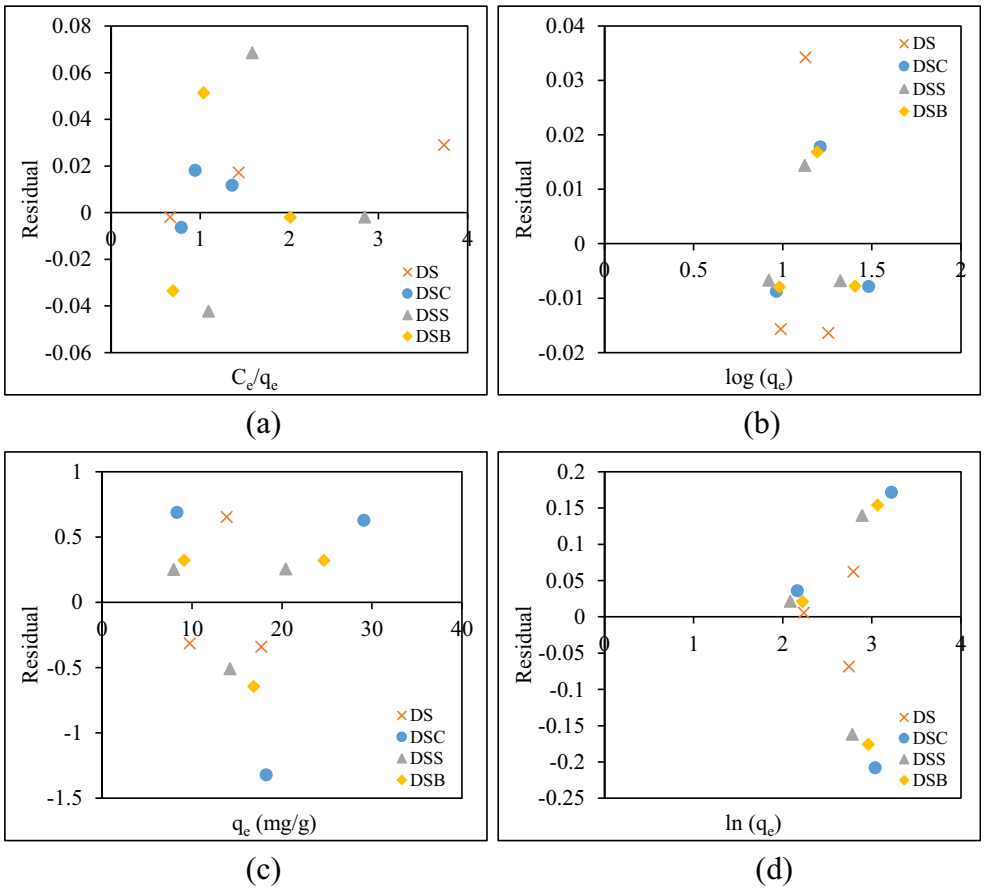

Fig. 5 Residual plots for linear isotherm models for sorption of RH dye on DS and carbonaceous materials: **a** Langmuir, **b** Freundlich, **c** Temkin, and **d** Dubinin-Radushkevich

was operated to assess the impact of pH, sorbent dosage, initial dye concentration, temperature, and contact time on RH dye removal (%). A matrix was created due to high and low levels of factors as given in Table 2, which were represented by 2 and 1, respectively. The experimental conditions were preferred according to well-known literature studies such as pH (2 and 8), biosorbent dosage (0.1 and 0.4 g/50 mL), initial concentration (50 and 100 mg/L), temperature (20 and 40 °C), and contact time (60 and 120 min).

2.6 Artificial neural networks

One of the main factors underlying the widespread use of ANNs is their ability to understand the complicated interactions between input variables efficiently. This property has enabled ANNs to be used in many different fields for generating predictions. Recent studies in the field of dye removal demonstrate that ANNs are capable of producing predictions with high accuracy. Ghaedi and Vafaei [71] have reviewed recent studies of the applications of ANNs in the area of adsorption science. To predict the dye removal efficiencies of *Daphne* seed–based sorbents over the various operating conditions, a three-layer feed-forward ANN with back-propagation was applied. This is because a three-layer feed-forward neural network with an appropriate back-propagation algorithm can solve any continuous function over a set of inputs approximately [72]. Also, ANNs are capable of generating accurate predictions when trained with a small amount of data [73]. Within the scope of the study, various ANN models with back-propagation algorithms were tested and compared: Levenberg-Marquardt (trainlm), resilient (trainrp), scaled conjugate gradient (trainscg), Polak-Ribiére conjugate gradient (traincpg), and variable learning rate gradient (traingdx). Training algorithms were also tested under different transfer functions: (i) purelin, tansig, and logsig for the hidden layer, and (ii) purelin for the output layer. The architecture of a three-layer feed-forward back-propagation model was schematized in Fig. 1 related to sorption parameters.

Feed-forward networks consist of a series of interconnected layers from the input layer to the last layer and do not contain any feedback connections. A feed-forward network with a single hidden layer can be applied to any finite input-output mapping problem if it has enough neurons in its hidden layer [74]. The usage of an incorrect amount of neurons in the hidden layer can prevent the ANN model from correctly generating predictions. The number of neurons in the hidden layer

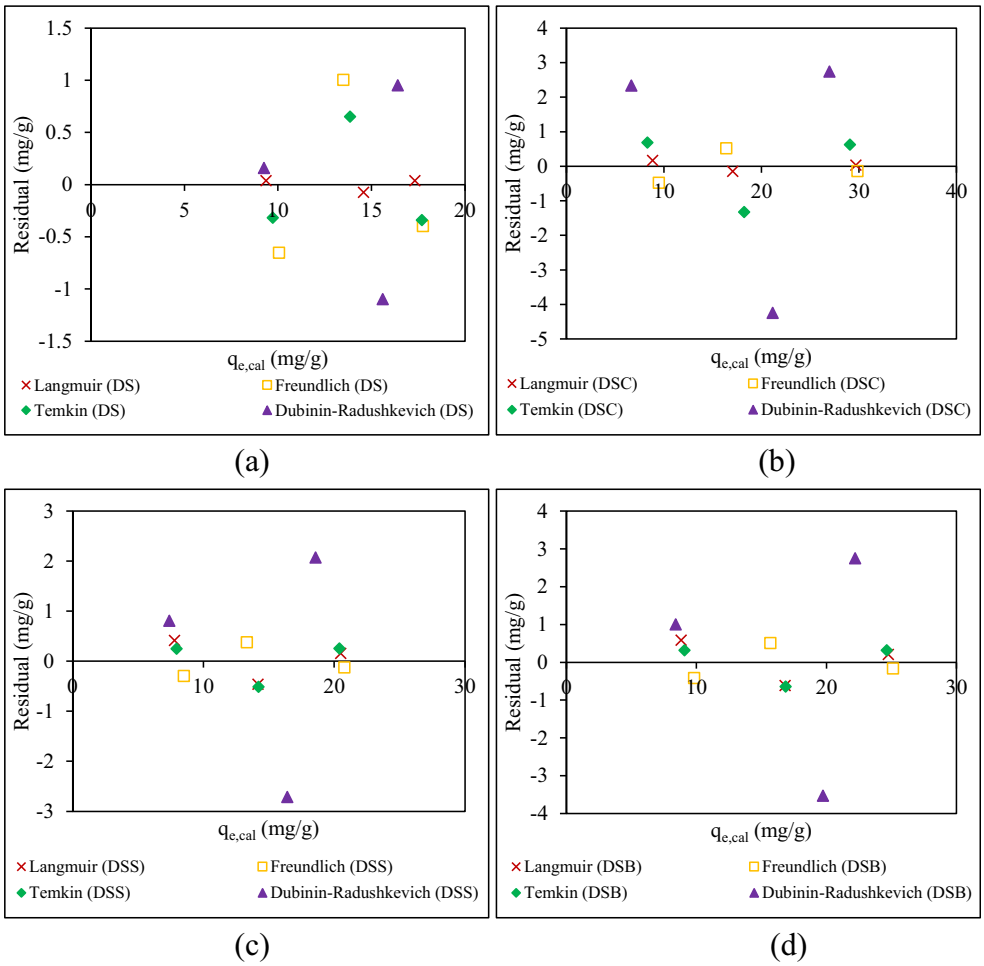

Fig. 6 Residual plots for non-linear isotherm models for sorption of RH dye on **a** DS, **b** DSC, **c** DSS, and **d** DSB

should be decided according to the properties of the data set and the difficulty of the problem. Although advanced computational techniques (i.e., genetic algorithm) [75] are used to determine the appropriate network architecture, trial and error method is frequently applied to specify the optimal number of neurons in the hidden layer [71, 73, 76–78]. Besides, there are some approaches to approximate the number of neurons. The range of neuron numbers for the hidden layer (Z_h) is limited by using Eq. (15) [79].

$$2\sqrt{Z_i} + Z_0 \leq Z_h \leq 2Z_i + 1 \tag{15}$$

where Z_i and Z_0 were denoted as the studied experimental conditions (pH, sorbent dosage, initial dye concentration, temperature, and contact time) and performance measures numbers (prediction of dye removal efficiency (%)), respectively. In this direction, the number of hidden layer nodes was examined in the range of 6–11.

The data sets used in dye removal process included 32 experimental runs for each sorbent (DS, DSC, DSB, and DSS). In order to reduce the effect of outliers on the prediction accuracy, the data set was normalized in the range of 0 to 1 according to Eq. (16):

$$x_{\text{new}} = x_i - \min(x)/\max(x) - \min(x) \tag{16}$$

where x_{new} is the normalized value of the input data x_i. The $\min(x)$ and $\max(x)$ represent the minimum and maximum values of the input data, respectively.

By performing the cross-validation procedure, it was ensured that each data in the data set was incorporated in the prediction generating process. The uncertainty caused by the random data selection for testing and training in the predictive performance of ANNs was minimized through this procedure. For this purpose, the data set was randomly split into k disjoint folds by applying the k-fold cross-validation procedure (k = 10). Each fold was tested by the model which was trained by using remaining k-1 folds. The prediction generation success of the model was determined by the average of the prediction accuracies obtained for each fold. ANNs' model performances were compared by using the coefficient of determination (R^2) and root mean squared error (RMSE). The optimum number of

Table 5 Sorption kinetic models constants and correlation coefficients for RH dye uptake

Model	Parameters	Sorbent type			
		DS	DSC	DSS	DSB
–	$q_{e,exp}$ (mg/g)	16.7	17.3	19.6	21.4
Pseudo-first order model					
Linear model	R^2	0.394	0.216	0.062	0.049
	$q_{e,cal}$ (mg/g)	6.25	3.22	2.24	3.91
	k_1 (min^{-1})	0.0184	0.0092	0.0023	0.0023
	RMSE	0.3674	0.4007	0.3140	0.2212
Non-linear model	R^2	0.982	0.961	0.944	0.944
	$q_{e,cal}$ (mg/g)	15.81	15.59	18.09	18.74
	k_1 (min^{-1})	0.0539	0.6373	0.1448	0.1322
	RMSE	0.7397	1.1151	1.5450	1.6068
Pseudo-second-order model					
Linear model	R^2	0.978	0.972	0.966	0.934
	$q_{e,cal}$ (mg/g)	17.54	17.54	19.61	20.00
	k_2 (g/mg·min)	0.0051	0.0382	0.0081	0.0094
	RMSE	0.3388	0.3872	0.3810	0.5329
Non-linear model	R^2	0.982	0.962	0.948	0.948
	$q_{e,cal}$ (mg/g)	17.70	15.82	18.69	19.44
	k_2 (g/mg·min)	0.0046	0.0763	0.0231	0.0189
	RMSE	0.7310	1.1021	1.4934	1.5409
Intraparticle diffusion model					
Linear model	R^2	0.726	0.198	0.188	0.211
	C	8.8801	13.822	15.503	15.816
	k_i (mg/g·$min^{0.5}$)	0.6709	0.2048	0.2833	0.3158
	RMSE	6.0986	0.9988	1.4265	1.4773
Non-linear model	R^2	0.842	0.676	0.680	0.687
	C	3.0096	4.6848	5.2544	5.3605
	k_i (mg/g·$min^{0.5}$)	1.3028	1.1883	1.3864	1.4412
	RMSE	2.1942	3.2013	3.6975	3.7808

hidden layer neurons, transfer functions, and training algorithms were determined among the created ANNs in MATLAB software (vR2019b).

3 Results and discussion

In this section, properties of *Daphne* seed and carbonaceous sorbents, statistical findings of color uptake, parameters of equilibrium, and kinetic investigations were examined.

3.1 Characteristics of sorbents

Proximate analysis of DS and ultimate analyses of all sorbents are given in Table 3. The *Daphne* seed content was ascertained as high in volatile matter and moisture. After carbonization method, the calorific value and carbon content improved considerably while the oxygen content reduced in the sample, which designated that DSC, DSB, and DSS were more carbonaceous material than DS. The bulk density of *Daphne* seed was 0.47 g/cm^3. The specific surface area and pore diameter of the DS were 0.26 m^2/g and 38.7 nm, respectively. The specific surface area and pore diameter of the carbonaceous material (DSC) produced without any activation process were obtained as 1.17 m^2/g and 36.6 nm, respectively. The addition of salt and base increased the surface area to 199.79 and 120.46 m^2/g as a result of the activation process. The average pore diameters were between 4.4 and 38.7 nm which indicated that sorbents were in the mesoporous region.

The FT-IR spectrum determines the chemical compositions and surface characteristics of the materials. FT-IR analysis was implemented to identify *Daphne* seed and carbonaceous sorbent's surface functional groups appertaining to bind RH dye. The FT-IR spectra of DS with many absorption peaks are presented in Fig. 2, which indicated the complex nature of the biosorbent. Functional groups of DSC and activated carbons are also seen in Fig. 2. O–H stretching vibration of hydroxyl functional groups involving hydrogen bonding was the primary functional group which was identified at bandwidths of 3300–3200 cm^{-1} [80]. C–H aliphatic symmetrical and asymmetrical stretching for methyl and methylene peaks was detected between 2950 and 2800 cm^{-1}. Peak detected at 1627 cm^{-1} indicated the aromatic C=C ring stretch. Peaks observed at 1442 cm^{-1} and 1370 cm^{-1} were constituted C–H stretching bands of aliphatic CH_3 groups. C–O–C stretching of unsaturated ethers was observed between 1275 and 1200 cm^{-1}, and also small bands ranging from 1200 to 1000 cm^{-1} were nominated as out-of-plane C–H bending of aromatic structures [81]. Peaks settled on bandwidths of 900–700 cm^{-1} could be attributed to substituents linked to an aromatic ring.

3.2 Kinetics, isotherms, and thermodynamic modeling

Fitting the sorption data to different isotherm models and the prediction of batch sorption kinetics are important steps to determine the suitable model for the design of sorption systems. In this part, the results of kinetic models and equilibrium isotherms were notified. Besides, thermodynamic parameters were calculated.

3.2.1 Adsorption isotherms

Adsorption isotherms were used to determine the affinity of *Daphne* seed and carbonaceous sorbents for RH dye. Freundlich, Langmuir, Dubinin-Radushkevich, and Temkin isotherms of RH dye uptake were achieved at pH 2 for 120 min. Initial dye concentrations

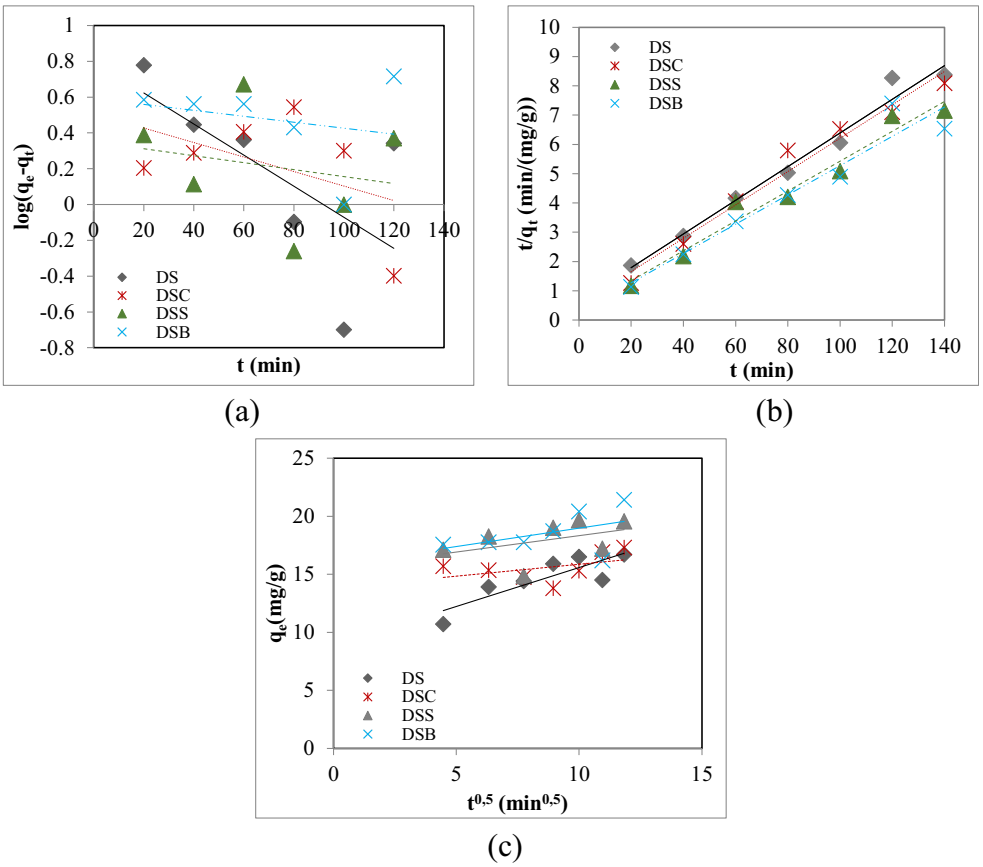

Fig. 7 Linear kinetic models for sorption of RH dye on DS-based sorbents: **a** pseudo-first-order, **b** pseudo-second-order, and **c** intraparticle diffusion

differentiated as 25, 50, and 100 mg/L; the temperature stayed constant at 40 °C. Sorption experimental data associated with the linear and non-linear forms of the isotherm models as well as all constants, R^2, and RMSE values are summarized in Table 4. Plots of C_e vs. C_e/q_e, $\log C_e$ vs. $\log q_e$, lnC_e vs. q_e, and ε^2 vs. lnq_e were shown in Fig. 3 for the linear forms of Langmuir, Freundlich, Temkin, and Dubinin-Radushkevich isotherm models, respectively. Plots of C_e vs. q_e were given for non-linear isotherm models in Fig. 4. The highest correlation coefficient (R^2 value) was achieved from Langmuir isotherm; hence, the Langmuir model demonstrated better fit to the sorption data than the other models, indicating thereby the monolayer sorption of the dye. The smallest RMSE values were obtained when the Langmuir isotherm model was applied to DS and DSC, while the Freundlich isotherm model gave the smallest RMSE values for DSS and DSB. Temkin isotherms display relatively high sorption potentials between the sorbents and RH dye ions. The value of B specifies whether the sorption is endothermic or exothermic: (i) If $B > 0$, the process is exothermic and the heat is released during the sorption process; (ii) if $B < 0$, the endothermic process takes place and the heat is absorbed during adsorption [82]. The Temkin model proved the exothermic nature of the sorption process with the positive B value which was the sign of released heat. To examine the physical and chemical mechanism of the sorption process, the energy term calculated from the Dubinin-Radushkevich model is utilized. The sorption mechanism is determined by evaluating the mean free energy (E, kJ/mol) in three intervals: (i) If $E < 8$ kJ/mol, the sorption is a physical process (physisorption) with Van der Waals interactions; (ii) If $8 < E < 16$ kJ/mol, sorption is controlled by ion exchange, more likely with the domination of covalent bond interactions; (iii) If $E > 16$ kJ/mol, the sorption occurs through particle diffusion [83, 84]. The linear form of Dubinin-Radushkevich model plots of lnq_e versus ε^2 for sorption of dye ions onto *Daphne*-based sorbents is given in Fig. 3d. Sorption energies of *Daphne*-based sorbents were found lower than the value of 8 kJ/mol, and indicated that the sorption of RH dye ions was a physisorption process. In the last step, the residual values of both linear and non-linear isotherm models were calculated and the residual plots are given in Figs. 5 and 6. According to the residual plots, the Dubinin-Radushkevich model among the both linear and non-linear isotherm models, with the highest difference between the experimental and fitted data, was not adequate to define the adsorption of RH dye on *Daphne*-based

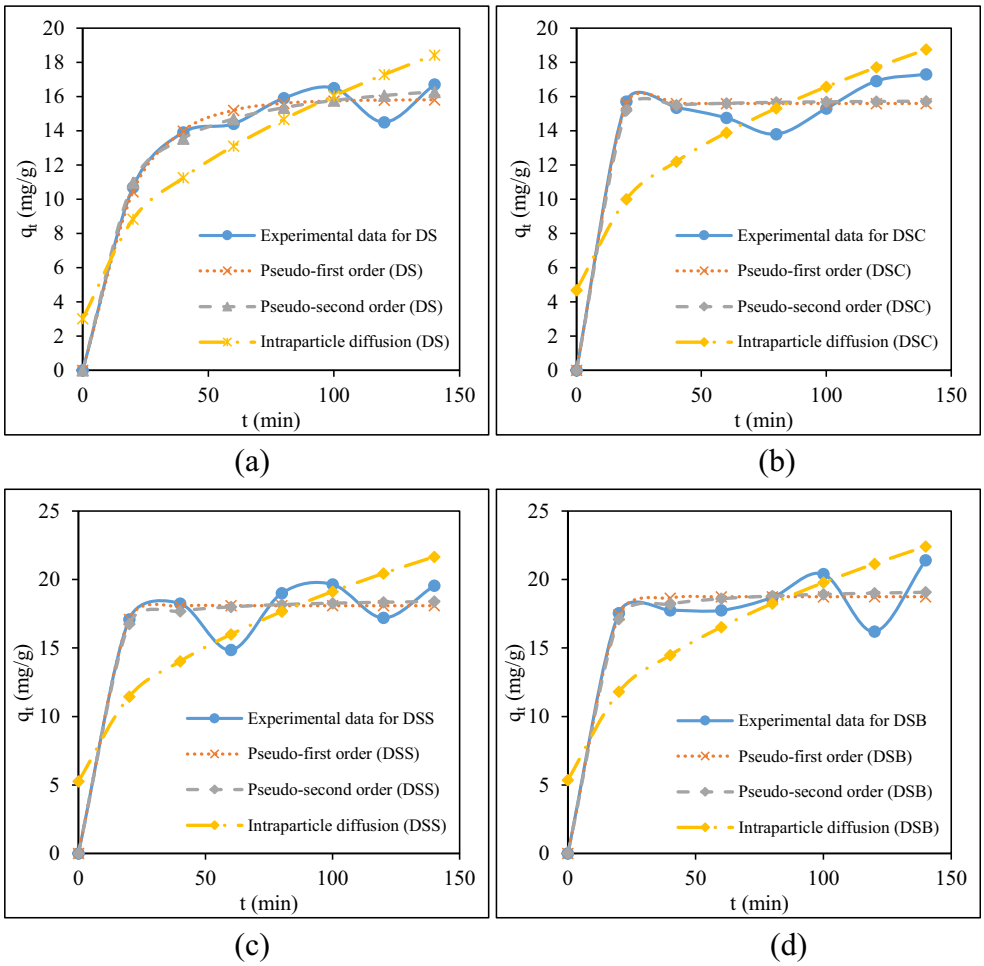

Fig. 8 Non-linear kinetic models for sorption of RH dye on **a** DS, **b** DSC, **c** DSS, and **d** DSB at 40 °C

sorbents. The residual plots of other isotherm models support that these models were sufficient to explain RH dye sorption.

3.2.2 Adsorption kinetics

Various kinetic models have been suggested to elucidate the mechanism of solute sorption from aqueous solution onto a sorbent. RH dye with a concentration of 50 mg/L at pH = 2 was eliminated at different periods at 40 °C. The adsorption rate constants (k_1, k_2, and k_i), q_e, correlation coefficient (R^2), and RMSE values were computed from the linear and non-linear plots (Figs. 7 and 8) and presented in Table 5. As shown in Table 5, the correlation coefficient (R^2) values for the pseudo-first-order and intraparticle diffusion models were not close to unity. A great change in the values of $q_{e,cal}$ and $q_{e,exp}$ for the sorption of RH dye onto DS and carbonaceous sorbents exposed that the pseudo-first-order model was not appropriate to define the kinetic profile of the sorption. According to this interpretation, it has been determined that the mechanism of chemisorption probably controlled the sorption via the pseudo-second-order kinetic model. The intraparticle diffusion model was used to study the rate-limiting step in the sorption process. If q_t versus $t^{0.5}$ displays a straight line passing through the origin, the sorption is dominated by intraparticle diffusion only [82]. As illustrated in Fig. 4c, the fitting curves did not pass through the origin, signifying that intraparticle diffusion was not the only rate-limiting step in the sorption process [85]. Finally, the residual values of both linear and non-linear kinetic models were considered and the residual plots are shown in Figs. 9 and 10. When the intraparticle diffusion model was applied between both linear and non-linear kinetic models, it was determined that the residual distribution around the zero axes was asymmetrical and error values (RMSE) were also higher than those of other models, and it was concluded that this model did not adequately describe the RH dye sorption process.

3.2.3 Adsorption thermodynamics

The thermodynamic parameters and Van't Hoff plot are given in Table 6 and Fig. 11, respectively. When the enthalpy change is positive, the sorption process takes place endothermically. The enthalpy change during the biosorption of RH dye onto the surface of *DS* was positive and the process was endothermic, while the adsorption processes on the

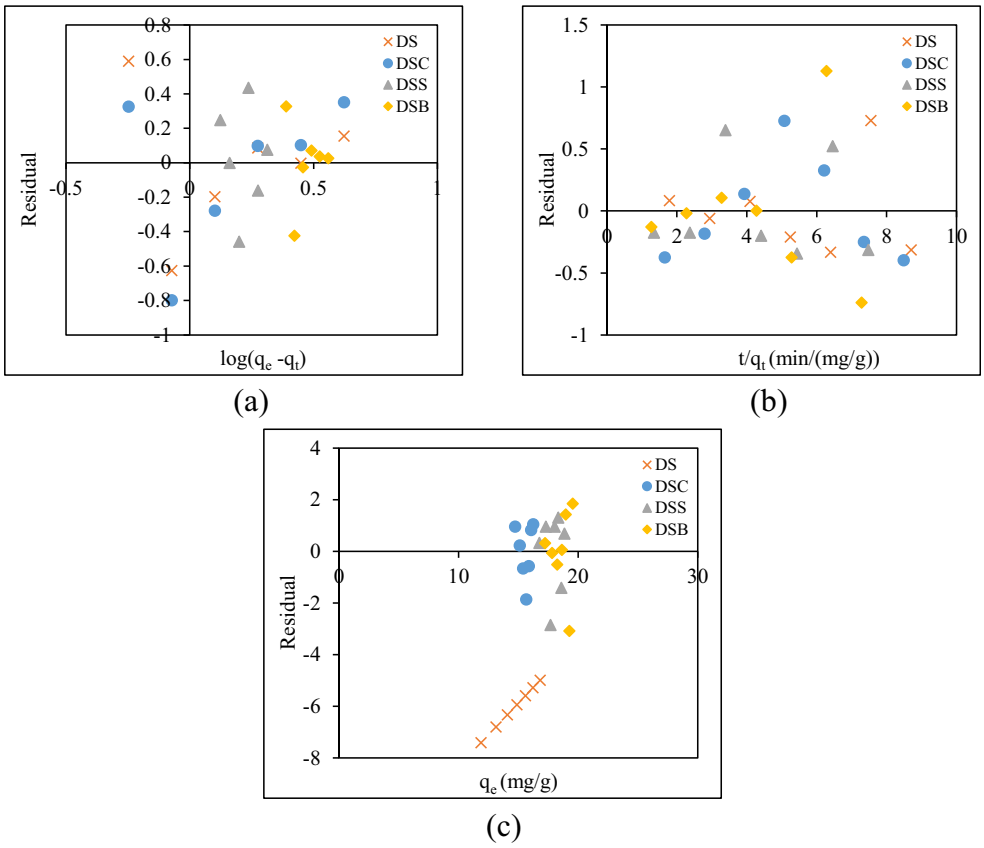

Fig. 9 Residual plots for the linear kinetic models for sorption of RH dye on DS-based sorbents: **a** pseudo-first-order, **b** pseudo-second-order, and **c** intraparticle diffusion

surface of other carbonaceous sorbents (DSC, DSS, and DSB) were exothermic. It is stated that the randomness at the adsorbent/solution interface decreases when the entropy change is negative, and the process is enthalpy driven. The positive entropy change was the sign of advancing the affinity of the DS for RH dye. The negative Gibbs free energy change indicates that the adsorption process is spontaneous. The Gibbs free energy change of carbonaceous sorbents tended to the positive values with the temperature rise; thus, the sorption process was favorable at lower temperatures.

3.3 Statistical factorial analysis

Two-level full factorial design (2^5) was operated for the modeling of sorption process. The effects along with the statistical plots (normal probability of standardized effects, Pareto charts, plots of main and interaction effects) and the statistical parameters were obtained by analyzing the experimental data with MINITAB 18 statistical software. The experimental design matrix that included coded values of variables is illustrated in Table 7. pH of solution (2 and 8), sorbent dosage (0.1 and 0.4 g/50 mL), contact time (60 and 120 min), initial dye concentration (50 and 100 mg/L), and temperature (20 and 40 °C) were variables in the design matrix. The number of runs was given by $a^k = 2^5 = 32$ where a and k were the count of levels and the number of factors [86]. The probability value (P value) is utilized to decide the statistically agents in the model, and the 95% confidence level is generally approved statistically significant. The analysis of variance (ANOVA) designated the interactions between independent variables, and the P value with > 95% of confidence level was selected to specify the main effects of dye sorption.

The relation between the experimental variables and corresponding responses is clarified by the subsequent equation:

$$\begin{aligned} Y = {} & X_0 + X_1A + X_2B + X_3C + X_4D + X_5E + X_6AB \\ & + X_7AC + X_8AD + X_9AE + X_{10}BC + X_{11}BD \\ & + X_{12}BE + X_{13}CD + X_{14}CE + X_{15}DE \\ & + X_{16}ABC + X_{17}ABD + X_{18}ABE + X_{19}ACD \\ & + X_{20}ACE + X_{21}ADE + X_{22}BCD + X_{23}BCE \\ & + X_{24}BDE + X_{25}CDE + X_{26}ABCD + X_{27}ABCE \\ & + X_{28}ABDE + X_{29}ACDE + X_{30}BCDE \end{aligned} \quad (17)$$

where Y is the predicted response (dye removal efficiency, %), X_0 signifies the global mean, and X_i symbolizes the regression coefficient related to the main factors' effects and interactions.

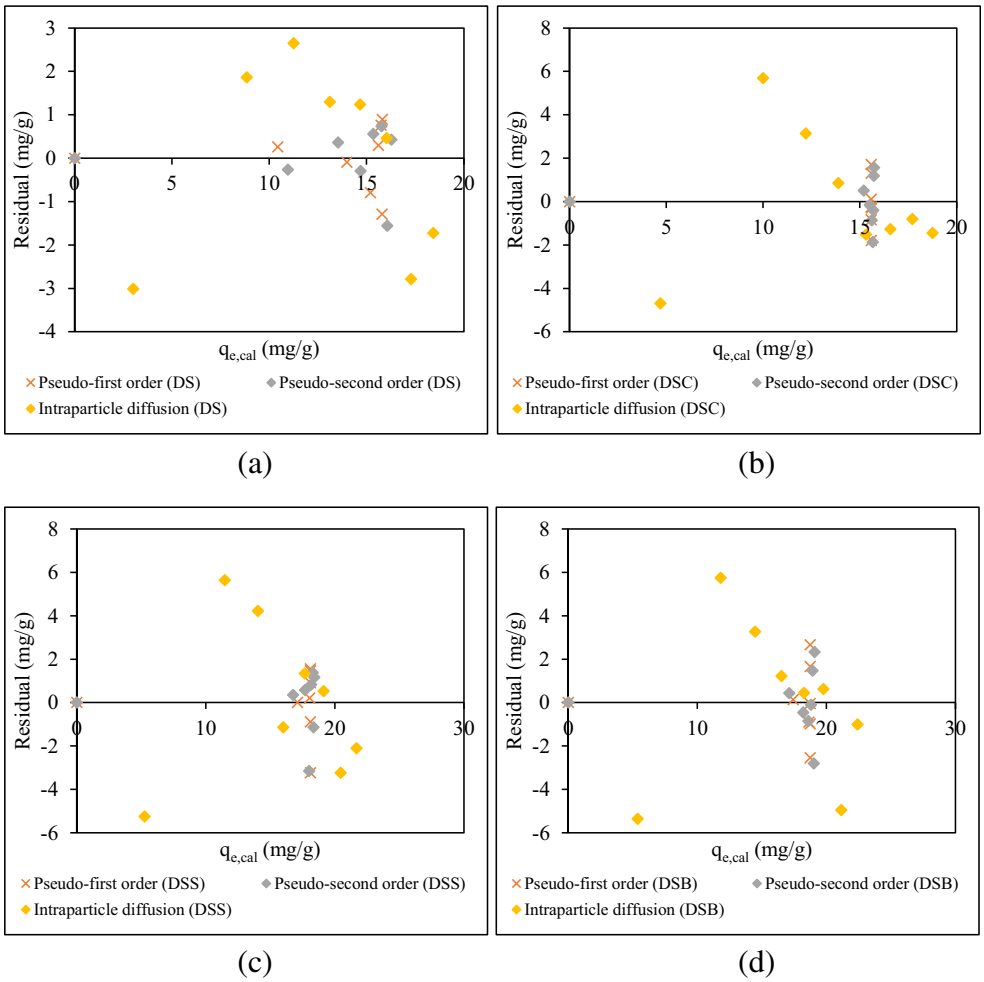

Fig. 10 Residual plots for the non-linear kinetic models for sorption of RH dye on **a** DS, **b** DSC, **c** DSS, and **d** DSB

A, *B*, *C*, *D*, and *E* stand for the solution pH, the sorbent dosage (g/50 mL), the temperature (°C), the contact time (min), and the initial dye concentration (mg/L), respectively.

Table 6 Thermodynamic parameters for RH dye sorption

Sorbent type	*T* (K)	ΔH° (kJ/mol)	ΔS° (J/molK)	ΔG° (kJ/mol)
DS	293	13.80	40.91	1.813
	303			1.404
	313			0.995
DSC	293	− 3.89	− 12.03	− 0.364
	303			− 0.244
	313			− 0.124
DSS	293	− 0.713	− 1.46	− 0.284
	303			− 0.269
	313			− 0.254
DSB	293	− 47.16	− 151.18	− 2.868
	303			− 1.356
	313			0.155

3.3.1 Analysis of variance

Univariate analysis of variance contributed a qualified and beneficial tool for statistical analyses of factors and their interactions in tests [87, 88]. The significant main and

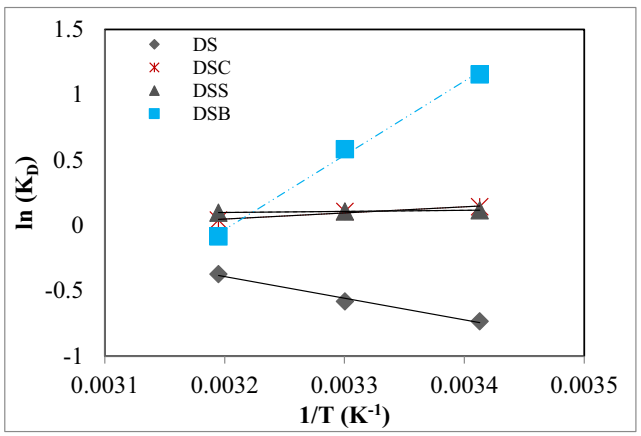

Fig. 11 Van't Hoff plot for the determination of thermodynamic parameters

Table 7 Experimental design matrix of RY sorption

Runs	Factors				
	A	*B*	*C*	*D*	*E*
1	− 1	− 1	− 1	− 1	− 1
2	− 1	− 1	− 1	− 1	1
3	− 1	− 1	− 1	1	− 1
4	− 1	− 1	− 1	1	1
5	− 1	− 1	1	− 1	− 1
6	− 1	− 1	1	− 1	1
7	− 1	− 1	1	1	− 1
8	− 1	− 1	1	1	1
9	− 1	1	− 1	− 1	− 1
10	− 1	1	− 1	− 1	1
11	− 1	1	− 1	1	− 1
12	− 1	1	− 1	1	1
13	− 1	1	1	− 1	− 1
14	− 1	1	1	− 1	1
15	− 1	1	1	1	− 1
16	− 1	1	1	1	1
17	1	− 1	− 1	− 1	− 1
18	1	− 1	− 1	− 1	1
19	1	− 1	− 1	1	− 1
20	1	− 1	− 1	1	1
21	1	− 1	1	− 1	− 1
22	1	− 1	1	− 1	1
23	1	− 1	1	1	− 1
24	1	− 1	1	1	1
25	1	1	− 1	− 1	− 1
26	1	1	− 1	− 1	1
27	1	1	− 1	1	− 1
28	1	1	− 1	1	1
29	1	1	1	− 1	− 1
30	1	1	1	− 1	1
31	1	1	1	1	− 1
32	1	1	1	1	1

Table 8 Statistical parameters for 2^5 design of RH removal by DS

Term	Effect	Coef	SE coef	*T*-value	*P* value
Constant		29.412	0.812	36.20	0.018
A	− 28.050	− 14.025	0.812	− 17.26	0.037
B	2.737	1.369	0.812	1.68	0.341
C	3.237	1.619	0.812	1.99	0.296
D	6.000	3.000	0.812	3.69	0.168
E	− 20.175	− 10.087	0.812	− 12.42	0.051
A*B	− 4.012	− 2.006	0.812	− 2.47	0.245
A*C	− 1.488	− 0.744	0.812	− 0.92	0.528
A*D	− 1.525	− 0.763	0.812	− 0.94	0.520
A*E	− 0.300	− 0.150	0.812	− 0.18	0.884
B*C	2.450	1.225	0.812	1.51	0.373
B*D	1.062	0.531	0.812	0.65	0.631
B*E	− 0.813	− 0.406	0.812	− 0.50	0.705
C*D	4.363	2.181	0.812	2.68	0.227
C*E	2.738	1.369	0.812	1.68	0.341
D*E	− 3.350	− 1.675	0.812	− 2.06	0.288
A*B*C	− 3.000	− 1.500	0.812	− 1.85	0.316
A*B*D	2.763	1.381	0.812	1.70	0.339
A*B*E	4.487	2.244	0.812	2.76	0.221
A*C*D	− 1.762	− 0.881	0.812	− 1.08	0.474
A*C*E	− 3.238	− 1.619	0.812	− 1.99	0.296
A*D*E	− 1.125	− 0.562	0.812	− 0.69	0.614
B*C*D	2.375	1.188	0.812	1.46	0.382
B*C*E	2.200	1.100	0.812	1.35	0.405
B*D*E	− 1.438	− 0.719	0.812	− 0.88	0.539
C*D*E	− 4.888	− 2.444	0.812	− 3.01	0.204
A*B*C*D	0.325	0.162	0.812	0.20	0.874
A*B*C*E	− 0.400	− 0.200	0.812	− 0.25	0.846
A*B*D*E	− 2.288	− 1.144	0.812	− 1.41	0.393
A*C*D*E	2.538	1.269	0.812	1.56	0.363
B*C*D*E	− 0.025	− 0.012	0.812	− 0.02	0.990

interaction effects of factors affecting the RH dye removal efficiency (%) were determined by applying the typical ANOVA. The ANOVA results of RH (main and interaction effects, the model coefficients, probability values and standard errors of every coefficient) are displayed in Tables 8, 9, 10, and 11. The sum of the squares exploited to evaluate factors' influence and Fisher's *F*-ratios and *P* values is even denoted in Tables 12, 13, 14, and 15.

ANOVA foresaw that the main factor of solution pH was greatly significant ($P < 0.05$) for all sorbents and the model was feasible for *Daphne* seed–based sorbents. Besides, the effect of sorbent dosage along with the pH effect for DSB sorbent was found to be significant ($P = 0.045$). Besides, the fit model notified square correlation coefficients (R^2) of 0.9981, 0.9985, 0.9971, and 0.9995 were harmonized with the statistical model for DS, DSC, DSS, and DSB, respectively. Four model equations obtained for RH dye removal efficiency (%) are specified in Eqs. (18–21). Resulting equations were achieved by subrogating the coefficients X_i in Eq. (17) by their values from Tables 8 to 11, respectively. If the effect of a factor on the response (η-dye removal efficiency) is also increased when its level changes from low to high values, the effect is considered to be positive. For instance, pH, initial concentration, pH-

temperature-contact time interaction, etc. were negative effects on RH dye removal via *DS* sorption.

$$\begin{aligned}\eta\ of\ \mathrm{DS} = {} & 29.412-14.025A + 1.369B + 1.619C \\ & + 3.000D-10.087E-2.006AB-0.744\ AC-0.763\ AD-0.150AE \\ & + 1.225\ BC + 0.531BD-0.406BE + 2.181CD \\ & + 1.369\ CE-1.675DE-1.500ABC + 1.381ABD \\ & + 2.244ABE-0.881ACD-1.619ACE-0.562ADE \\ & + 1.188BCD + 1.100\ BCE-0.719BDE-2.444CDE \\ & + 0.162ABCD-0.200ABCE-1.144ABDE \\ & + 1.269ACDE-0.012BCDE \end{aligned} \quad (18)$$

$$\begin{aligned}\eta\ of\ \mathrm{DSC} = {} & 39.79-25.81A + 4.22B + 1.31C \\ & + 4.66D-3.85E-0.11AB + 2.94\ AC \\ & + 2.37\ AD + 1.30AE + 2.72\ BC \\ & + 3.87BD + 1.13BE + 3.59CD-0.35\ CE \\ & + 0.80DE + 2.34ABC + 3.91ABD \\ & + 1.96ABE + 3.40ACD-0.93ACE \\ & + 1.06ADE + 0.72BCD-1.54\ BCE \\ & + 0.66BDE-1.15CDE \\ & + 2.43ABCD-1.82ABCE \\ & + 0.14ABDE-2.34ACDE-0.62BCDE \end{aligned} \quad (19)$$

$$\begin{aligned}\eta\ of\ \mathrm{DSS} = {} & 47.67-15.81A + 7.85B-1.22C \\ & + 0.24D-6.03E + 2.16AB \\ & + 4.97\ AC-0.07\ AD + 1.99AE + 1.63\ BC \\ & + 0.64BD-0.93BE + 1.49CD + 0.08\ CE \\ & + 2.99DE-1.10ABC-1.19ABD-0.46ABE \\ & + 2.29ACD + 2.97ACE \\ & + 0.28ADE-0.33BCD-1.75\ BCE \\ & + 0.66BDE + 0.69CDE + 1.16ABCD \\ & + 0.48ABCE-0.21ABDE-0.31ACDE \\ & + 0.25BCDE \end{aligned} \quad (20)$$

$$\begin{aligned}\eta\ of\ \mathrm{DSB} = {} & 48.044-22.650A \\ & + 8.762B-0.737C-0.781D-3.156E \\ & + 1.969AB + 3.081\ AC-5.813\ AD + 0.150AE \\ & + 1.419\ BC-2.025BD + 5.538BE-3.975CD \\ & + 1.713\ CE + 0.544DE-1.563ABC-3.856ABD \\ & -0.456ABE-2.544ACD + 2.281ACE-0.337ADE \\ & -2.656BCD + 3.394\ BCE-0.575BDE \\ & + 0.550CDE-4.175ABCD + 2.463ABCE \\ & -0.656ABDE + 0.481ACDE-1.856BCDE \end{aligned} \quad (21)$$

Table 9 Statistical parameters for 2^5 design of RH removal by DSC

Term	Effect	Coef	SE coef	*T*-value	*P* value
Constant		39.79	1.11	35.97	0.018
A	− 51.62	− 25.81	1.11	− 23.33	0.027
B	8.44	4.22	1.11	3.81	0.163
C	2.62	1.31	1.11	1.19	0.446
D	9.33	4.66	1.11	4.21	0.148
E	− 7.70	− 3.85	1.11	− 3.48	0.178
A*B	− 0.21	− 0.11	1.11	− 0.10	0.939
A*C	5.88	2.94	1.11	2.66	0.229
A*D	4.75	2.37	1.11	2.15	0.278
A*E	2.60	1.30	1.11	1.18	0.449
B*C	5.44	2.72	1.11	2.46	0.246
B*D	7.74	3.87	1.11	3.50	0.177
B*E	2.26	1.13	1.11	1.02	0.493
C*D	7.18	3.59	1.11	3.24	0.190
C*E	− 0.70	− 0.35	1.11	− 0.32	0.805
D*E	1.60	0.80	1.11	0.72	0.601
A*B*C	4.69	2.34	1.11	2.12	0.281
A*B*D	7.81	3.91	1.11	3.53	0.176
A*B*E	3.91	1.96	1.11	1.77	0.328
A*C*D	6.80	3.40	1.11	3.07	0.200
A*C*E	− 1.85	− 0.93	1.11	− 0.84	0.557
A*D*E	2.12	1.06	1.11	0.96	0.513
B*C*D	1.44	0.72	1.11	0.65	0.633
B*C*E	− 3.09	− 1.54	1.11	− 1.40	0.396
B*D*E	1.31	0.66	1.11	0.59	0.659
C*D*E	− 2.30	− 1.15	1.11	− 1.04	0.488
A*B*C*D	4.86	2.43	1.11	2.20	0.272
A*B*C*E	− 3.64	− 1.82	1.11	− 1.64	0.348
A*B*D*E	0.29	0.14	1.11	0.13	0.918
A*C*D*E	− 4.68	− 2.34	1.11	− 2.11	0.281
B*C*D*E	− 1.24	− 0.62	1.11	− 0.56	0.675

Table 10 Statistical parameters for 2^5 design of RH removal by DSS

Term	Effect	Coef	SE coef	*T*-value	*P* value
Constant		47.67	1.11	42.85	0.015
A	− 31.61	− 15.81	1.11	− 14.21	0.045
B	15.70	7.85	1.11	7.06	0.090
C	− 2.44	− 1.22	1.11	− 1.10	0.471
D	0.49	0.24	1.11	0.22	0.863
E	− 12.06	− 6.03	1.11	− 5.42	0.116
A*B	4.32	2.16	1.11	1.94	0.302
A*C	9.94	4.97	1.11	4.47	0.140
A*D	− 0.14	− 0.07	1.11	− 0.06	0.961
A*E	3.99	1.99	1.11	1.79	0.324
B*C	3.25	1.63	1.11	1.46	0.382
B*D	1.28	0.64	1.11	0.57	0.669
B*E	− 1.85	− 0.93	1.11	− 0.83	0.558
C*D	2.99	1.49	1.11	1.34	0.408
C*E	0.16	0.08	1.11	0.07	0.954
D*E	5.99	2.99	1.11	2.69	0.227
A*B*C	− 2.20	− 1.10	1.11	− 0.99	0.504
A*B*D	− 2.37	− 1.19	1.11	− 1.07	0.479
A*B*E	− 0.92	− 0.46	1.11	− 0.42	0.749
A*C*D	4.59	2.29	1.11	2.06	0.287
A*C*E	5.94	2.97	1.11	2.67	0.228
A*D*E	0.56	0.28	1.11	0.25	0.842
B*C*D	− 0.65	− 0.33	1.11	− 0.29	0.819
B*C*E	− 3.50	− 1.75	1.11	− 1.57	0.360
B*D*E	1.33	0.66	1.11	0.60	0.658
C*D*E	1.39	0.69	1.11	0.62	0.645
A*B*C*D	2.33	1.16	1.11	1.04	0.486
A*B*C*E	0.95	0.48	1.11	0.43	0.743
A*B*D*E	− 0.42	− 0.21	1.11	− 0.19	0.880
A*C*D*E	− 0.61	− 0.31	1.11	− 0.28	0.829
B*C*D*E	0.50	0.25	1.11	0.22	0.859

Table 11 Statistical parameters for 2^5 design of RH removal by DSB

Term	Effect	Coef	SE coef	*T*-value	*P* value
Constant		48.044	0.625	76.87	0.008
A	− 45.300	− 22.650	0.625	− 36.24	0.018
B	17.525	8.762	0.625	14.02	0.045
C	− 1.475	− 0.737	0.625	− 1.18	0.448
D	− 1.563	− 0.781	0.625	− 1.25	0.430
E	− 6.312	− 3.156	0.625	− 5.05	0.124
A*B	3.938	1.969	0.625	3.15	0.196
A*C	6.163	3.081	0.625	4.93	0.127
A*D	− 11.625	− 5.813	0.625	− 9.30	0.068
A*E	0.300	0.150	0.625	0.24	0.850
B*C	2.838	1.419	0.625	2.27	0.264
B*D	− 4.050	− 2.025	0.625	− 3.24	0.191
B*E	11.075	5.538	0.625	8.86	0.072
C*D	− 7.950	− 3.975	0.625	− 6.36	0.099
C*E	3.425	1.713	0.625	2.74	0.223
D*E	1.087	0.544	0.625	0.87	0.544
A*B*C	− 3.125	− 1.563	0.625	− 2.50	0.242
A*B*D	− 7.713	− 3.856	0.625	− 6.17	0.102
A*B*E	− 0.912	− 0.456	0.625	− 0.73	0.599
A*C*D	− 5.087	− 2.544	0.625	− 4.07	0.153
A*C*E	4.562	2.281	0.625	3.65	0.170
A*D*E	− 0.675	− 0.337	0.625	− 0.54	0.685
B*C*D	− 5.312	− 2.656	0.625	− 4.25	0.147
B*C*E	6.787	3.394	0.625	5.43	0.116
B*D*E	− 1.150	− 0.575	0.625	− 0.92	0.527
C*D*E	1.100	0.550	0.625	0.88	0.541
A*B*C*D	− 8.350	− 4.175	0.625	− 6.68	0.095
A*B*C*E	4.925	2.463	0.625	3.94	0.158
A*B*D*E	− 1.313	− 0.656	0.625	− 1.05	0.484
A*C*D*E	0.962	0.481	0.625	0.77	0.582
B*C*D*E	− 3.713	− 1.856	0.625	− 2.97	0.207

3.3.2 Normal probability plots of standardized effects and Pareto charts

The distribution of data is graphically represented by the normal probability plot [89]; one point on the plot is nominated for each effect. If the points on the plot scatter properly pretty well a straight line, formerly normally distributed data are observed [90]. The normal probability plots of standardized effects are given in Fig. 12. The standardized effects are t-statistics that verify the null hypothesis that the effect is 0. The experimental points were acceptably aligned signifying normal distribution. Whole points of normal probability plots were arisen to rank in the range of + 5 to − 20 for DS, + 5 to − 25 for DSC, + 10 to − 15 for DSS, and + 15 to − 40 for DSB. Normal distribution recommended that the model designated a nominal deviation at the fitted value from the observed value [91]. The factors are specified positive coefficients on the right part of normal probability plots. Despite that, the factors are identified as negative coefficients on the left part of the chart. Significant and insignificant factors and interactions are symbolized as a circle and a square, respectively.

The Pareto chart of the standardized effects (Fig. 13) illuminated the comparative significance of the individual and interaction effects. The certain values of the standardized effects are given in the Pareto chart from the largest effect to the smallest effect. For a 0.05 probability and one degree of freedom, value was equal to 12.71. Effects positioned at right side of the vertical dash line were significant; pH of the dye solution was the supreme variable of all sorption processes.

Table 12 Analysis of variance (ANOVA) for DS

Source	DF	Adj SS	Adj MS	*F*-value	*P* value
Model	30	11312.6	377.09	17.85	0.185
Linear	5	9982.5	1996.49	94.51	0.078
A	1	6294.4	6294.42	297.96	0.037
B	1	60.0	59.95	2.84	0.341
C	1	83.9	83.85	3.97	0.296
D	1	288.0	288.00	13.63	0.168
E	1	3256.2	3256.25	154.14	0.051
2-way interactions	10	530.1	53.01	2.51	0.458
A*B	1	128.8	128.80	6.10	0.245
A*C	1	17.7	17.70	0.84	0.528
A*D	1	18.6	18.60	0.88	0.520
A*E	1	0.7	0.72	0.03	0.884
B*C	1	48.0	48.02	2.27	0.373
B*D	1	9.0	9.03	0.43	0.631
B*E	1	5.3	5.28	0.25	0.705
C*D	1	152.3	152.25	7.21	0.227
C*E	1	60.0	59.95	2.84	0.341
D*E	1	89.8	89.78	4.25	0.288
3-way interactions	10	704.5	70.45	3.33	0.404
A*B*C	1	72.0	72.00	3.41	0.316
A*B*D	1	61.1	61.05	2.89	0.339
A*B*E	1	161.1	161.10	7.63	0.221
A*C*D	1	24.9	24.85	1.18	0.474
A*C*E	1	83.9	83.85	3.97	0.296
A*D*E	1	10.1	10.13	0.48	0.614
B*C*D	1	45.1	45.13	2.14	0.382
B*C*E	1	38.7	38.72	1.83	0.405
B*D*E	1	16.5	16.53	0.78	0.539
C*D*E	1	191.1	191.10	9.05	0.204
4-way interactions	5	95.5	19.10	0.90	0.659
A*B*C*D	1	0.8	0.84	0.04	0.874
A*B*C*E	1	1.3	1.28	0.06	0.846
A*B*D*E	1	41.9	41.86	1.98	0.393
A*C*D*E	1	51.5	51.51	2.44	0.363
B*C*D*E	1	0.0	0.00	0.00	0.990
Error	1	21.1	21.12		
Total	31	11333.7			

S = 4.59619 R-Sq = 99.81% R-Sq(adj) = 94.22%

Table 13 Analysis of variance (ANOVA) for DSC

Source	DF	Adj SS	Adj MS	*F*-value	*P* value
Model	30	26671.1	889.0	22.70	0.165
Linear	5	23115.7	4623.1	118.05	0.070
A	1	21321.1	21321.1	544.44	0.027
B	1	569.5	569.5	14.54	0.163
C	1	55.1	55.1	1.41	0.446
D	1	695.6	695.6	17.76	0.148
E	1	474.3	474.3	12.11	0.178
2-way interactions	10	1703.7	170.4	4.35	0.358
A*B	1	0.4	0.4	0.01	0.939
A*C	1	276.1	276.1	7.05	0.229
A*D	1	180.5	180.5	4.61	0.278
A*E	1	54.1	54.1	1.38	0.449
B*C	1	236.5	236.5	6.04	0.246
B*D	1	479.0	479.0	12.23	0.177
B*E	1	41.0	41.0	1.05	0.493
C*D	1	411.8	411.8	10.52	0.190
C*E	1	3.9	3.9	0.10	0.805
D*E	1	20.5	20.5	0.52	0.601
3-way interactions	10	1368.8	136.9	3.50	0.396
A*B*C	1	175.8	175.8	4.49	0.281
A*B*D	1	488.3	488.3	12.47	0.176
A*B*E	1	122.5	122.5	3.13	0.328
A*C*D	1	369.9	369.9	9.45	0.200
A*C*E	1	27.4	27.4	0.70	0.557
A*D*E	1	36.1	36.1	0.92	0.513
B*C*D	1	16.5	16.5	0.42	0.633
B*C*E	1	76.3	76.3	1.95	0.396
B*D*E	1	13.8	13.8	0.35	0.659
C*D*E	1	42.3	42.3	1.08	0.488
4-way interactions	5	482.8	96.6	2.47	0.448
A*B*C*D	1	189.2	189.2	4.83	0.272
A*B*C*E	1	105.9	105.9	2.70	0.348
A*B*D*E	1	0.7	0.7	0.02	0.918
A*C*D*E	1	174.8	174.8	4.46	0.281
B*C*D*E	1	12.3	12.3	0.31	0.675
Error	1	39.2	39.2		
Total	31	26710.3			

S = 6.25790 R-Sq = 99.85% R-Sq(adj) = 95.45%

3.3.3 Main effects and interaction effects

The primary changes arisen in the response when the levels of the factors were changed from an inferior level to a higher level are shown in Fig. 14. This change is commonly termed the main effect as it denotes the main factor of concern with the experiment [92]. When the factor's effect is negative, the response (dye removal efficiency, %) reduces as the factor replaces from low to high levels. Inversely, if the effect is positive, response increases from lower level to higher level [93]. The extent of the vertical line demonstrates the statistical implication of a factor in such a way that the greater the vertical line in main effect plots is the superior the adjustment in dye removal efficiency (%) between lower and higher levels. The *ABCDE* effect was not significant when compared to other effects. The rise in the pH

Table 14 Analysis of variance (ANOVA) for DSS

Source	DF	Adj SS	Adj MS	*F*-value	*P* value
Model	30	13461.9	448.73	11.33	0.232
Linear	5	11180.2	2236.04	56.46	0.101
A	1	7994.8	7994.80	201.86	0.045
B	1	1971.9	1971.92	49.79	0.090
C	1	47.5	47.53	1.20	0.471
D	1	1.9	1.90	0.05	0.863
E	1	1164.0	1164.03	29.39	0.116
2-way interactions	10	1550.3	155.03	3.91	0.376
A*B	1	149.6	149.64	3.78	0.302
A*C	1	790.0	790.03	19.95	0.140
A*D	1	0.2	0.15	0.00	0.961
A*E	1	127.2	127.20	3.21	0.324
B*C	1	84.5	84.50	2.13	0.382
B*D	1	13.0	13.01	0.33	0.669
B*E	1	27.4	27.38	0.69	0.558
C*D	1	71.4	71.40	1.80	0.408
C*E	1	0.2	0.21	0.01	0.954
D*E	1	286.8	286.80	7.24	0.227
3-way interactions	10	674.4	67.44	1.70	0.539
A*B*C	1	38.7	38.72	0.98	0.504
A*B*D	1	45.1	45.12	1.14	0.479
A*B*E	1	6.8	6.84	0.17	0.749
A*C*D	1	168.4	168.36	4.25	0.287
A*C*E	1	282.0	282.03	7.12	0.228
A*D*E	1	2.5	2.53	0.06	0.842
B*C*D	1	3.4	3.38	0.09	0.819
B*C*E	1	98.0	98.00	2.47	0.360
B*D*E	1	14.0	14.05	0.35	0.658
C*D*E	1	15.4	15.40	0.39	0.645
4-way interactions	5	56.9	11.38	0.29	0.879
A*B*C*D	1	43.2	43.25	1.09	0.486
A*B*C*E	1	7.2	7.22	0.18	0.743
A*B*D*E	1	1.4	1.45	0.04	0.880
A*C*D*E	1	3.0	3.00	0.08	0.829
B*C*D*E	1	2.0	2.00	0.05	0.859
Error	1	39.6	39.60		
Total	31	13501.5			

S = 6.29325 R-Sq = 99.71% R-Sq(adj) = 90.91%

Table 15 Analysis of variance (ANOVA) for DSB

Source	DF	Adj SS	Adj MS	*F*-value	*P* value
Model	30	24960.7	832.0	66.56	0.097
Linear	5	19229.4	3845.9	307.67	0.043
A	1	16416.7	16416.7	1313.34	0.018
B	1	2457.0	2457.0	196.56	0.045
C	1	17.4	17.4	1.39	0.448
D	1	19.5	19.5	1.56	0.430
E	1	318.8	318.8	25.50	0.124
2-way interactions	10	3295.5	329.5	26.36	0.151
A*B	1	124.0	124.0	9.92	0.196
A*C	1	303.8	303.8	24.30	0.127
A*D	1	1081.1	1081.1	86.49	0.068
A*E	1	0.7	0.7	0.06	0.850
B*C	1	64.4	64.4	5.15	0.264
B*D	1	131.2	131.2	10.50	0.191
B*E	1	981.2	981.2	78.50	0.072
C*D	1	505.6	505.6	40.45	0.099
C*E	1	93.8	93.8	7.51	0.223
D*E	1	9.5	9.5	0.76	0.544
3-way interactions	10	1552.5	155.2	12.42	0.218
A*B*C	1	78.1	78.1	6.25	0.242
A*B*D	1	475.9	475.9	38.07	0.102
A*B*E	1	6.7	6.7	0.53	0.599
A*C*D	1	207.1	207.1	16.56	0.153
A*C*E	1	166.5	166.5	13.32	0.170
A*D*E	1	3.6	3.6	0.29	0.685
B*C*D	1	225.8	225.8	18.06	0.147
B*C*E	1	368.6	368.6	29.48	0.116
B*D*E	1	10.6	10.6	0.85	0.527
C*D*E	1	9.7	9.7	0.77	0.541
4-way interactions	5	883.3	176.7	14.13	0.199
A*B*C*D	1	557.8	557.8	44.62	0.095
A*B*C*E	1	194.0	194.0	15.52	0.158
A*B*D*E	1	13.8	13.8	1.10	0.484
A*C*D*E	1	7.4	7.4	0.59	0.582
B*C*D*E	1	110.3	110.3	8.82	0.207
Error	1	12.5	12.5		
Total	31	24973.2			

S = 3.53553 R-Sq = 99.95% R-Sq(adj) = 98.45%

caused a remarkable reduction of RH removal by sorbents. Furthermore, removal efficiency (%) reduced with rising the initial dye concentration; this was because of the saturation of surface area and active sites of sorbent at higher concentrations [13, 70, 94]. In contrast, sorbent dosage, temperature, and contact time were found as positive effects that η improved with increasing the levels of these effects for DS and DSC sorbents. Initial dye concentration influenced RH dye sorption negatively for all type sorbents.

While the main effects provided a distinct knowledge, the interaction between two parameters would approve a superior expression of the process. The probable negative and positive two-variable interactions through the factors *A*, *B*, *C*, *D*, and *E* for η are exhibited in Fig. 15. Impressions of interaction between the two factors are observed in the non-parallel lines of

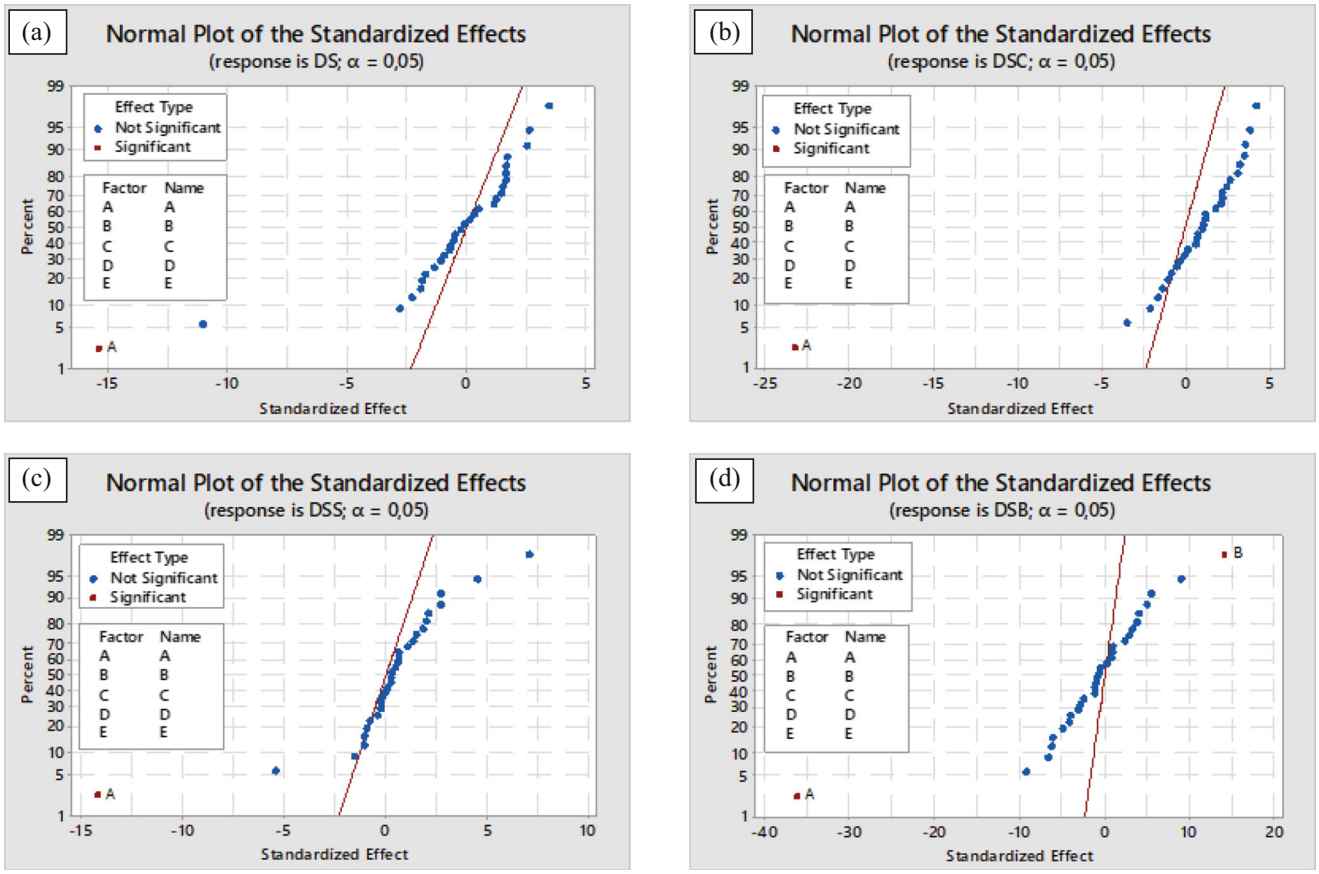

Fig. 12 Normal probability plots of standardized effects for η of **a** DS, **b** DSC, **c** DSS, and **d** DSB

the figure. These plots briefly indicated that interactions between pH and other factors (*AB*, *AC*, AD, and *AE*) were stronger than apart from these effects (*BC*, *BD*, *BE*, *CD*, *CE*, and *DE*).

3.4 Prediction results of ANN models

Various ANN models were created to predict the effectiveness of *Daphne* seed–based sorbents in Pr Red Hegxl dye removal. For each data set, combinations of various training algorithms (traincgp, traingdx, trainlm, trainrp, and trainscg) and transfer functions (tansig, logsig, and purelin for the hidden layer and purelin transfer function for the output layer) were used to determine the ANN model with the highest predictive accuracy. Each of the models was tested with 5 to 11 neurons in their hidden layers. In summary, a total of 90 ANN models were established to predict the dye removal efficiency (%) with high accuracy. To analyze the resulting accuracies of the created ANNs, the *k*-fold cross-validation approach (with $k = 10$) was used. As it is known, ANNs act like a "black box" [95]; therefore, the error coefficients obtained from the created models differ from each repetition. Therefore, the experiments were repeated ten times and the best of the obtained error coefficients was presented as the final result.

The prediction success of the created models was tested separately for each data set and the optimal network structure was determined by performance indices of R^2, and RMSE. Based on the evaluated training algorithms, the models with the highest prediction accuracy level for each data set are illustrated in Table 16. According to the comparison made by concerning R^2 values in the prediction results, each data set was examined separately:

- Among the ANN models proposed for the DS sorbent, the model with 5-8-1 structure produced the most satisfactory results ($R^2 = 0.999567$) with lower error values (RMSE = 0.002489). In this model, the network training algorithm and the activation function for the hidden layer were traincgp and tansig, respectively. The optimum number of neurons in the hidden layer of this model is determined as 8. Besides, the combination of traingdx training algorithm with tansig activation function showed the second-best performance in the testing step, with an R^2 value of 0.999325.
- For the DSC sorbent, it was observed that the Levenberg-Marquardt training algorithm (trainlm) gave the highest R^2 value (0.999836) with tansig activation function in the hidden layer in accordance with the model 5-10-1

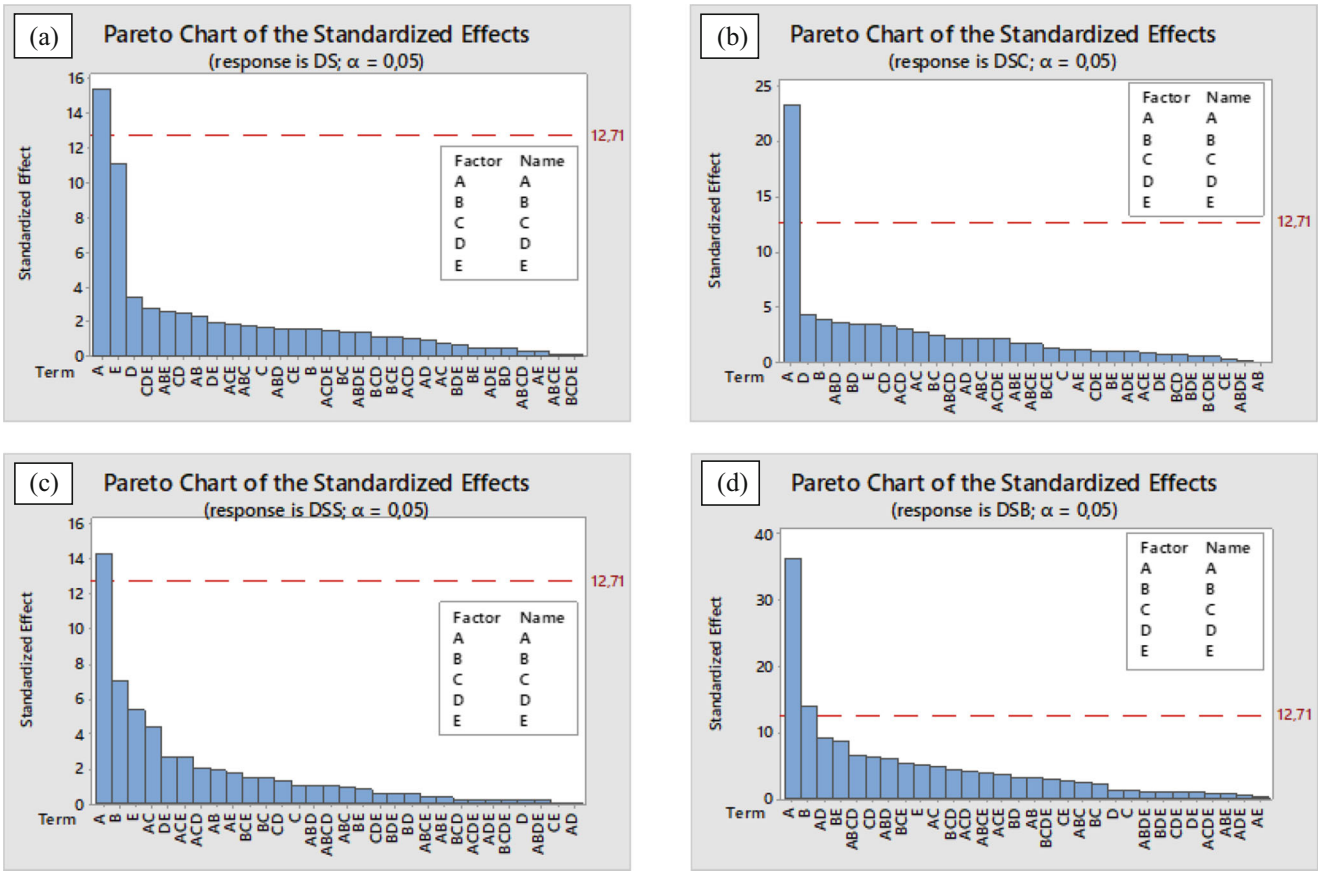

Fig. 13 Pareto charts for RH dye removal via **a** DS, **b** DSC, **c** DSS, and **d** DSB sorptions

structure. The RMSE value of this model was found as 0.001702.

- For DSS, which was evaluated as the third sorbent, the highest R^2 value was calculated as 0.997309 as a result of using traingdx training algorithm and tansig activation function together. The number of hidden layer neurons of the best ANN model created for this sorbent was specified as 11, and also the RMSE value was calculated as 0.004627.
- Similar to DSS, in ANN models created for the last sorbent DSB, traingdx training algorithm and tansig activation function produced the highest prediction accuracy (R^2 = 0.995872) with an acceptable RMSE value of 0.011384. It was designated that the most effective result was obtained for this model by using 10 neurons in the hidden layer.

The ANN models created using traincgp, traingdx, trainlm, trainrp, and trainscg training algorithms succeeded in predicting the effectiveness of *Daphne* seed–based sorbents in Pr Red Hegxl dye removal. It was concluded that the models created using the trainrp training algorithm within these structures produced relatively higher error rates than others. For example, the R^2 and RMSE error coefficients of the trainrp training algorithm for the DSS sorbent data set were 0.968080 and 0.031746, respectively. This model had the highest error rate among optimum ANN models which were presented based on the training algorithm in Table 16. Besides, it was determined that R^2 values were greater than 0.99 in all other ANN models except trainscg training algorithm–based model of the DSS sorbent data set. Finally, when RMSE values were examined, it was noticed that the ANN models with the highest error coefficient were created by using trainrp and trainscg training algorithms.

When the effect of the transfer functions used in the hidden layers on the prediction accuracy was examined, it was seen that the purelin transfer function–based models could produce predictions with higher error coefficients than sigmoidal (tansig and logsig) functions via back-propagation training algorithms; thus, the purelin transfer function was not included in the optimum models presented in Table 16.

Another important parameter to create the optimum structure in ANN models is the number of neurons used in the hidden layer. For the optimum models given in Table 16, the effect of the number of neurons used in the hidden layer on the prediction accuracy was examined separately for each

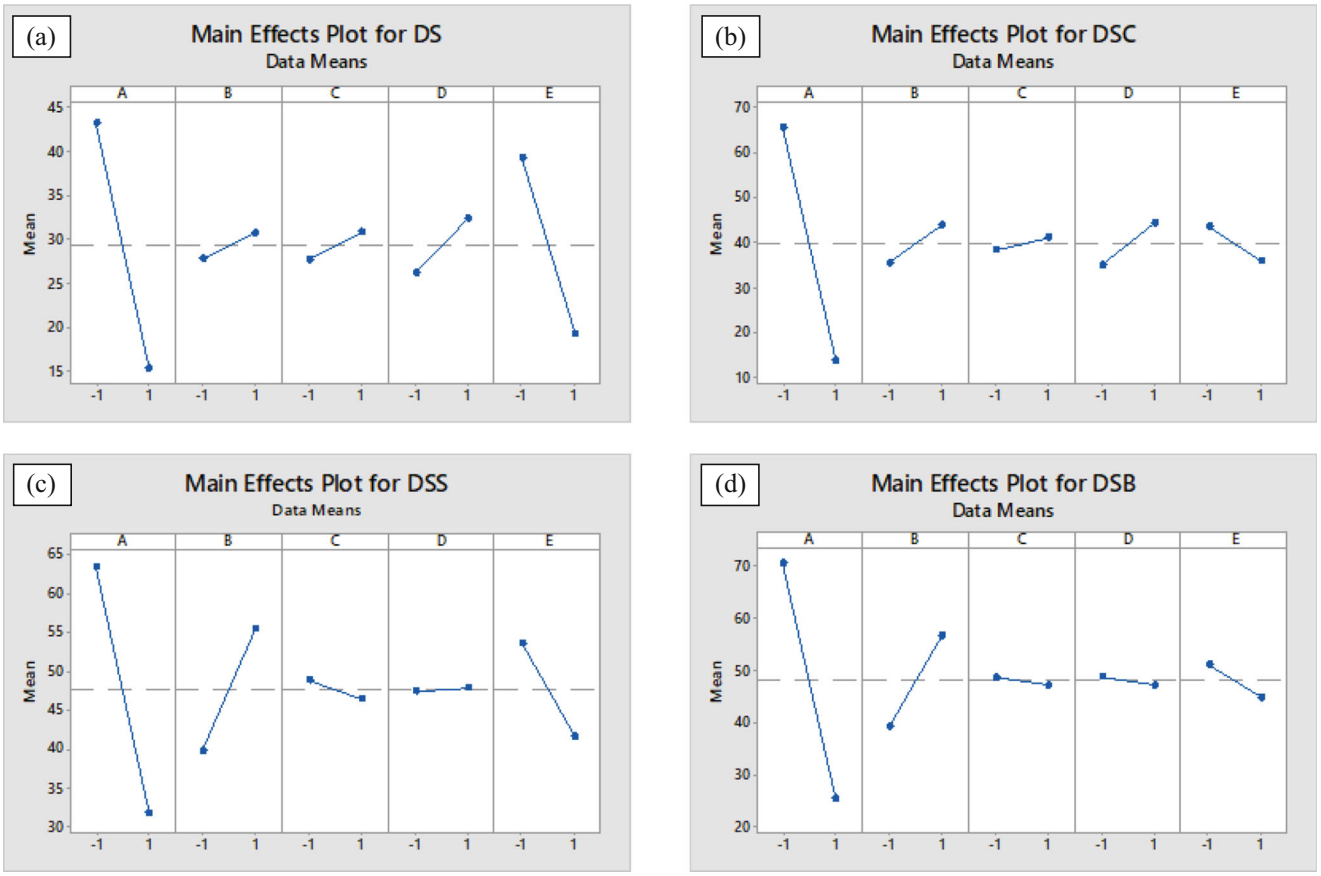

Fig. 14 Main effects plots for η of **a** DS, **b** DSC, **c** DSS, and **d** DSB sorptions

data set. The R^2 values obtained when the number of hidden layer neurons was changed in the range of 6–11 are given in Fig. 16. In order to validate the network performance, a linear regression was performed between the network outputs and the corresponding targets. The regression plots of the most accurate network models for each sorbent are displayed in Fig. 17 concerning the targets for testing data. R values were found above 0.99 for all data sets, and it was determined that there was a reasonably good fit.

4 Conclusion

Daphne seed is a favorable sorbent for the uptake of Pr Red Hegxl dye from aqueous solutions. The optimization of RH dye uptake employing DS, DSC, DSS, and DSB as sorbents were investigated through 2^5 full factorial experimental design to keep away from conventional one-factor-at-a-time experiments. The effects of pH, sorbent dosage, initial dye concentration, temperature, and contact time on %removal efficiency were designated. This optimization exposed that the best initial conditions for DS and DSC were as follows: pH 2, sorbent dosage 0.4 g/50 mL, temperature 40 °C, and initial dye concentration 50 mg/L with 70.8% and 83.2% removal efficiencies, respectively. The optimum contact time for sorption was 120 min for biomass and 60 min for char. The highest RH dye uptake values for DSS and DSB sorbents were obtained at 85.40% and 90.80% when lower pH and higher sorbent dosage levels were utilized. The optimization process established that the dye removal was enhanced by decreasing pH and initial dye concentration. pH was found to be the most significant factor due to the ANOVA results within a 95% confidence level. Also, artificial neural networks were tested for their ability to predict the reactive dye removal efficiency of *Daphne* seed–based sorbents from aqueous solutions. It was determined that the prediction accuracy of the created models was influenced by the number of neurons in the hidden layer, transfer functions, and training algorithms. Therefore, useful models with high accuracy ($R^2 > 0.97$ and RMSE < 0.031746) were obtained for each sorbent by testing various ANN structures created with combinations of traincgp, traingdx, trainlm, trainrp, and trainscg backpropagation algorithms and transfer functions (tansig, logsig, and purelin for the hidden layer and purelin activation function for the layer output). The sorption equilibrium was defined by using both linear and non-linear Freundlich, Langmuir, Temkin, and Dubinin-Radushkevich isotherm models, and the typical parameters of these models were

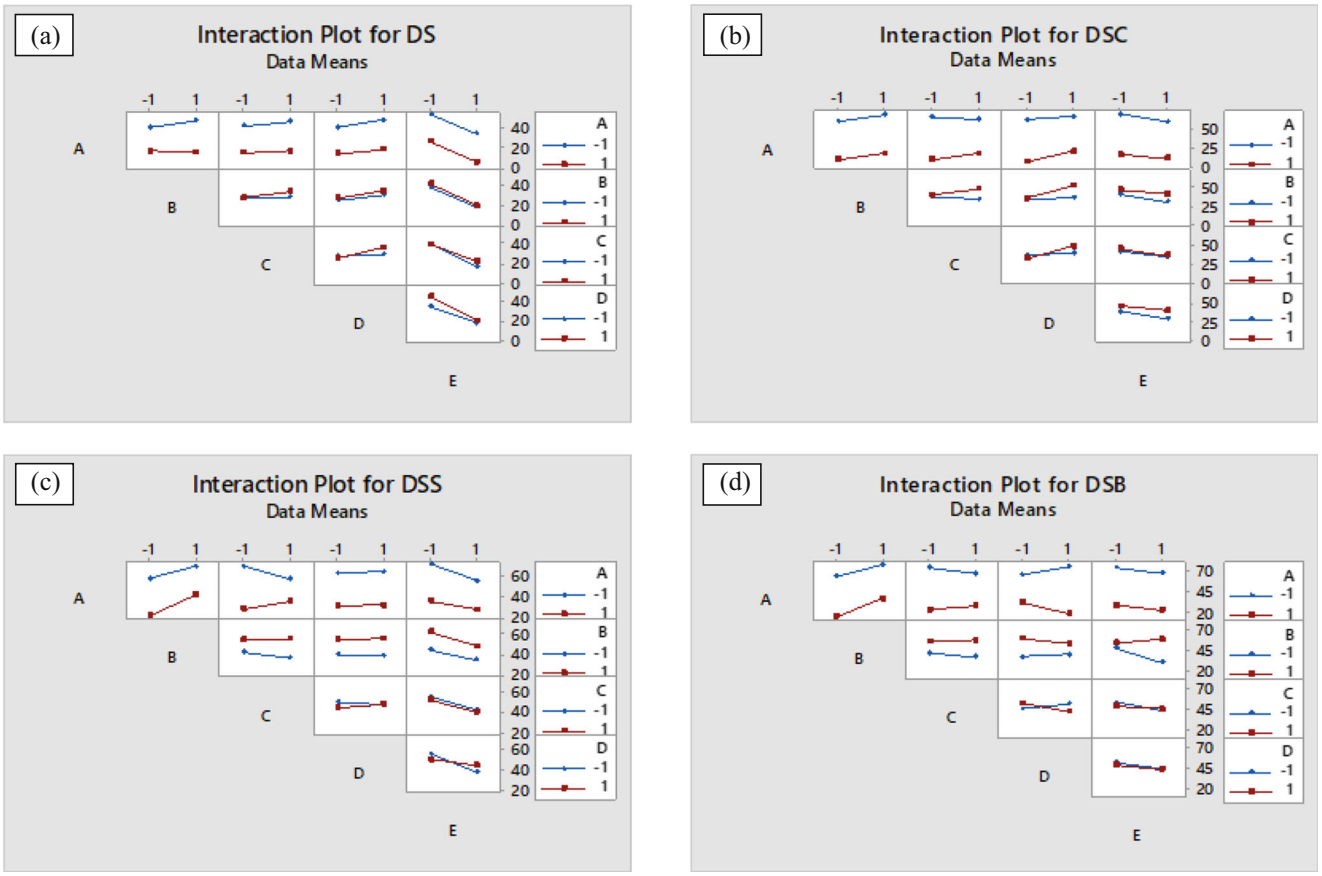

Fig. 15 Interaction effects plots for η of **a** DS, **b** DSC, **c** DSS, and **d** DSB sorptions

specified. The experimental data fitted the Langmuir model preferable than the other isotherms, which indicated homogeneous sorption of RH dye occurred. Sorption kinetics were examined by pseudo-first-order, pseudo-second-order, and intraparticle diffusion kinetic models; hereunder, the sorption process was controlled by chemical sorption due to the

Table 16 Testing results of ANN models to predict the removal efficiency (%) of *Daphne* seed–based sorbents

Sorption data sets	Network training function	Activation function for hidden layer	Optimal network structure	RMSE	R^2
DS	traincgp	tansig	5-8-1	0.002489	0.999567
	traingdx	tansig	5-8-1	0.004449	0.999325
	trainlm	tansig	5-10-1	0.004435	0.998341
	trainrp	logsig	5-6-1	0.012530	0.993809
	trainscg	logsig	5-9-1	0.002553	0.998975
DSC	traincgp	logsig	5-10-1	0.007961	0.997964
	traingdx	tansig	5-8-1	0.009881	0.998112
	trainlm	tansig	5-10-1	0.001702	0.999836
	trainrp	logsig	5-8-1	0.023624	0.993486
	trainscg	tansig	5-7-1	0.010297	0.997665
DSS	traincgp	tansig	5-11-1	0.004809	0.996783
	traingdx	tansig	5-11-1	0.004627	0.997309
	trainlm	logsig	5-8-1	0.008028	0.993375
	trainrp	logsig	5-10-1	0.031746	0.968080
	trainscg	tansig	5-9-1	0.015751	0.983699
DSB	traincgp	logsig	5-11-1	0.010024	0.995112
	traingdx	tansig	5-10-1	0.011384	0.995872
	trainlm	tansig	5-9-1	0.009897	0.995320
	trainrp	logsig	5-8-1	0.029110	0.984515
	trainscg	logsig	5-10-1	0.017914	0.991668

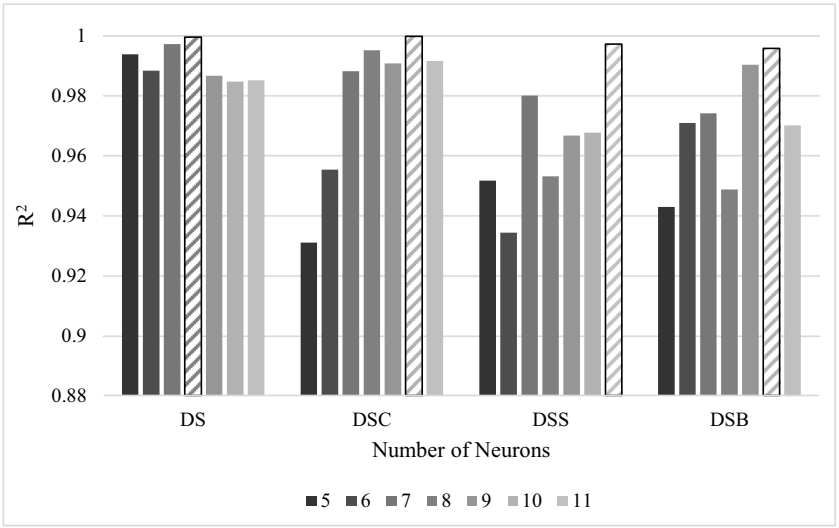

Fig. 16 The R^2 values versus the number of hidden layer neurons

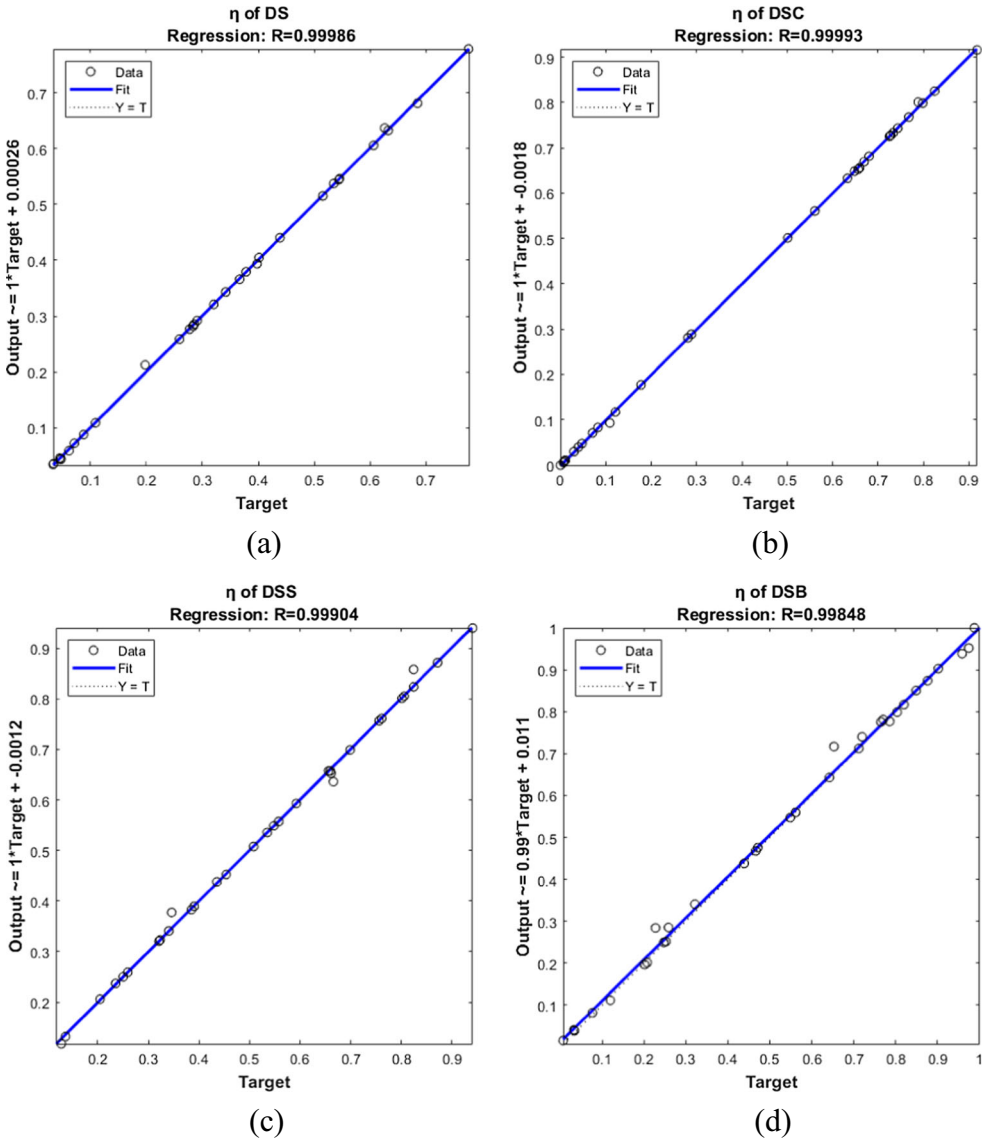

Fig. 17 Regression analysis for the neural network responses and the target for testing data: η of **a** DS, **b** DSC, **c** DSS, and **d** DSB

pseudo-second-order pathway. As a result, *Daphne* seed and carbonaceous sorbents can be good candidates to cleanse water bodies contaminated with such hazardous dyes. With the use of *Daphne*-based sorbents for dye removal, it was determined that high removal efficiency values up to 90% were achieved. It is noteworthy that this plant is used as an alternative sorbent in addition to its handling as a renewable energy source and chemical feedstock. When considering that the wild-growing *Daphne* is cultivated in Turkey, the utilization of domestic resources as a precursor for various purposes is economically attractive.

Authors' Contributions All authors contributed to the study conception and design. Material preparation, data collection, and optimization analysis were performed by Adife Seyda YARGIC. Prediction generation with ANNs was studied by Alper YARGIC. The first draft of the manuscript was written by Adife Seyda YARGIC and Alper YARGIC; all authors read and approved the final manuscript.

Compliance with ethical standards

Conflict of interest The authors declare that they have no conflict of interest.

References

1. Elfarash A, Mawad AM, Yousef NM, Shoreit AA (2017) Azoreductase kinetics and gene expression in the synthetic dyes-degrading Pseudomonas. Egyptian J Basic Appl Sci 4(4):315–322
2. Pengthamkeerati P, Satapanajaru T, Singchan O (2008) Sorption of reactive dye from aqueous solution on biomass fly ash. J Hazard Mater 153(3):1149–1156
3. Sathishkumar P, Arulkumar M, Palvannan T (2012) Utilization of agro-industrial waste Jatropha curcas pods as an activated carbon for the adsorption of reactive dye Remazol Brilliant Blue R (RBBR). J Clean Prod 22(1):67–75
4. Ahmad MA, Rahman NK (2011) Equilibrium, kinetics and thermodynamic of Remazol Brilliant Orange 3R dye adsorption on coffee husk-based activated carbon. Chem Eng J 170:154–161
5. Al-Degs YS, El-Barghouthi MI, El-Sheikh AH, Walker GM (2008) Effect of solution pH, ionic strength, and temperature on adsorption behavior of reactive dyes on activated carbon. Dyes Pigments 77(1):16–23
6. Geethakarthi A, Phanikumar BR (2011) Adsorption of reactive dyes from aqueous solutions by tannery sludge developed activated carbon: kinetic and equilibrium studies. Int J Environ Sci Technol 8(3):561–570
7. Garg VK, Gupta R, Yadav AB, Kumar R (2003) Dye removal from aqueous solution by adsorption on treated sawdust. Bioresour Technol 89(2):121–124
8. Elkady MF, Ibrahim AM, Abd El-Latif MM (2011) Assessment of the adsorption kinetics, equilibrium and thermodynamic for the potential removal of reactive red dye using eggshell biocomposite beads. Desalination 278:412–423
9. Namasivayam C, Kavitha D (2002) Removal of Congo Red from water by adsorption onto activated carbon prepared from coir pith, an agricultural solid waste. Dyes Pigments 54(1):47–58
10. Van HT, Nguyen TMP, Thao VT, Vu XH, Nguyen TV, Nguyen LH (2018) Applying activated carbon derived from coconut shell loaded by silver nanoparticles to remove methylene blue in aqueous solution. Water Air Soil Pollut 229(12):393
11. Daneshvar E, Vazirzadeh A, Niazi A, Kousha M, Naushad M, Bhatnagar A (2017) Desorption of Methylene blue dye from brown macroalga: effects of operating parameters, isotherm study and kinetic modeling. J Clean Prod 152:443–453
12. Jóźwiak T, Filipkowska U, Szymczyk P, Rodziewicz J, Mielcarek A (2017) Effect of ionic and covalent crosslinking agents on properties of chitosan beads and sorption effectiveness of Reactive Black 5 dye. React Funct Polym 114:58–74
13. Ozbay N, Yargic AS (2015) Factorial experimental design for Remazol Yellow dye sorption using apple pulp/apple pulp carbon–titanium dioxide co-sorbent. J Clean Prod 100:333–343
14. Wawrzkiewicz M, Bartczak P, Jesionowski T (2017) Enhanced removal of hazardous dye form aqueous solutions and real textile wastewater using bifunctional chitin/lignin biosorbent. Int J Biol Macromol 99:754–764
15. Suteu D, Badeanu M, Malutan T, Chirculescu AI (2016) Valorization of food wastes (orange seeds) as adsorbent for dye retention from aqueous medium. Desalination Water Treat 57(60):29070–29081
16. Kumar PS, Sivaprakash S, Jayakumar N (2017) Removal of Methylene Blue dye from aqueous solutions Using Lagerstroemia indica seed (LIS) activated carbon. Int J Mater Sci 12(1):107–116
17. Zhou K, Zhang Q, Wang B, Liu J, Wen P, Gui Z, Hu Y (2014) The integrated utilization of typical clays in removal of organic dyes and polymer nanocomposites. J Clean Prod 81:281–289
18. Uddin MT, Rahman MA, Rukanuzzaman M, Islam MA (2017) A potential low cost adsorbent for the removal of cationic dyes from aqueous solutions. Appl Water Sci:1–12
19. Yargıç AŞ, Yarbay Şahin RZ, Özbay N, Önal E (2014) Assessment of toxic copper(II) biosorption from aqueous solution by chemically-treated tomato waste (Solanum lycopersicum). J Clean Prod 88:152–159
20. Deniz F, Kepekci RA (2017) Bioremoval of Malachite green from water sample by forestry waste mixture as potential biosorbent. Microchem J 132:172–178
21. Mahmoud MS, Mostafa MK, Mohamed SA, Sobhy NA, Nasr M (2017) Bioremediation of red azo dye from aqueous solutions by Aspergillus niger strain isolated from textile wastewater. J Environ Chem Eng 5(1):547–554
22. Reddy MCS, Sivaramakrishna L, Reddy AV (2012) The use of an agricultural waste material, jujuba seeds for the removal of anionic dye (Congo red) from aqueous medium. J Hazard Mater 203-204: 118–127
23. Mustafa MM, Jamal P, Alkhatib MAF, Mahmod SS, Jimat DN, Ilyas NN (2017) Panus tigrinus as a potential biomass source for Reactive Blue decolorization: isotherm and kinetic study. Electron J Biotechnol 26:7–11
24. Gupta VK, Jain R, Varshney S (2007) Removal of Reactofix golden yellow 3 RFN from aqueous solution using wheat husk—an agricultural waste. J Hazard Mater 142:443–448
25. Salazar-Rabago JJ, Leyva-Ramos R, Rivera-Utrilla J, Ocampo-Perez R, Cerino-Cordova FJ (2017) Biosorption mechanism of Methylene Blue from aqueous solution onto White Pine (Pinus durangensis) sawdust: effect of operating conditions. Sustain Environ Res 27(1):32–40
26. Zaidi NAHM, Lim LB, Priyantha N, Usman A (2018) Artocarpus odoratissimus leaves as an eco-friendly adsorbent for the removal of toxic Rhodamine B dye in aqueous solution: equilibrium isotherm, kinetics, thermodynamics and regeneration studies. Arab J Sci Eng: 1–10
27. Seghier A, Hadjel M, Benderdouche N (2017) Adsorption study of heavy metal and acid dye on an amphoteric biomaterial using barbary fig skin. Arab J Sci Eng 42(4):1487–1496

28. Seghier A, Hadjel M, Benderdouche N (2018) Comparative study of the sorption capacity and contact time of Congo Red removal in a binary and singular system. Arab J Sci Eng 1-9
29. Menkiti MC, Aniagor CO (2018) Parametric studies on descriptive isotherms for the uptake of crystal violet dye from aqueous solution onto lignin-rich adsorbent. Arab J Sci Eng 43(5):2375–2392
30. Tang X, Tang P, Liu L (2018) Preparation of tetraethylenepentamine modified magnetic graphene oxide for adsorption of dyes from aqueous solution. J Braz Chem Soc 29(2): 334–342
31. Khalid A, Zubair M (2018) A comparative study on the adsorption of Eriochrome Black T dye from aqueous solution on graphene and acid-modified graphene. Arab J Sci Eng 43(5):2167–2179
32. Mohammed MI, Baytak S (2016) Synthesis of bentonite–carbon nanotube nanocomposite and its adsorption of rhodamine dye from water. Arab J Sci Eng 41(12):4775–4785
33. Elgarahy AM, Elwakeel KZ, Elshoubaky GA, Mohammad SH (2019) Microwave-accelerated sorption of cationic dyes onto green marine algal biomass. Environ Sci Pollut Res 26(22):22704–22722
34. Ncibi MC, Mahjoub B, Seffen M (2007) Adsorptive removal of textile reactive dye using Posidonia oceanica (L.) fibrous biomass. Int J Environ Sci Technol 4(4):433–440
35. Kousha M, Tavakoli S, Daneshvar E, Vazirzadeh A, Bhatnagar A (2015) Central composite design optimization of Acid Blue 25 dye biosorption using shrimp shell biomass. J Mol Liq 207:266–273
36. Inyinbor AA, Adekola FA, Olatunji GA (2015) Adsorption of Rhodamine B dye from aqueous solution on Irvingia gabonensis biomass: kinetics and thermodynamics studies. S Afr J Chem 68: 115–125
37. Ong ST, Keng PS, Lee SL, Leong MH, Hung YT (2010) Equilibrium studies for the removal of basic dye by sunflower seed husk (Helianthus annuus). Int J Phys Sci 5(8):1270
38. Nethaji S, Sivasamy A (2011) Adsorptive removal of an acid dye by lignocellulosic waste biomass activated carbon: equilibrium and kinetic studies. Chemosphere 82(10):1367–1372
39. Suteu D, Zaharia C, Malutan T (2011) Removal of orange 16 reactive dye from aqueous solutions by waste sunflower seed shells. J Serbian Chem Soc 76(4):607–624
40. Pathania D, Sharma A, Siddiqi ZM (2016) Removal of congo red dye from aqueous system using Phoenix dactylifera seeds. J Mol Liq 219:359–367
41. Reddy MS, Nirmala V, Ashwini C (2017) Bengal Gram Seed Husk as an adsorbent for the removal of dye from aqueous solutions–Batch studies. Arab J Chem 10:S2554–S2566
42. Machrouhi A, Farnane M, Elhalil A, Elmoubarki R, Abdennouri M, Qourzal S, Tounsadi H, Barka N (2018) Effectiveness of beetroot seeds and H3PO4 activated beetroot seeds for the removal of dyes from aqueous solutions. J Water Reuse Desalination 8(4):522–531
43. Daoud M, Benturki O, Kecira Z, Girods P, Donnot A (2017) Removal of reactive dye (BEZAKTIV Red S-MAX) from aqueous solution by adsorption onto activated carbons prepared from date palm rachis and jujube stones. J Mol Liq 243:799–809
44. Dawood S, Sen TK, Phan C (2014) Synthesis and characterisation of novel-activated carbon from waste biomass pine cone and its application in the removal of congo red dye from aqueous solution by adsorption. Water Air Soil Pollut 225(1):1818
45. Kumar KV, Kumaran A (2005) Removal of methylene blue by mango seed kernel powder. Biochem Eng J 27(1):83–93
46. Jóźwiak T, Filipkowska U, Brym S, Kopeć L (2020) Use of aminated hulls of sunflower seeds for the removal of anionic dyes from aqueous solutions. Int J Environ Sci Technol 17(3):1211–1224
47. Marzouki H, Piras A, Marongiu B, Rosa A, Dessi MA (2008) Extraction and separation of volatile and fixed oils from berries of Laurus nobilis L. by supercritical CO_2. Molecules 13(8):1702–1711
48. Beis SH, Dunford NT (2006) Supercritical fluid extraction of daphne (Laurus nobilis L.) seed oil. J Am Oil Chem Soc 83(11):953–957
49. Onay Ö (2012) Fast Pyrolysis of Laurel (Laurus Nobilis L.) Seed in a fixed-bed tubular reactor. Proceedings of the 55th International Convention of Society of Wood Science and Technology, Beijing, August 27-31.
50. Elkiran O, Akbaba E, Bagci E (2018) Constituents of essential oils from leaves and seeds of Laurus nobilis L.: a chemotaxonomic approach. Bangladesh J Bot 47(4):893–901
51. Onay Ö (2014) Effects of catalyst on pyrolysis of laurel (Laurus nobilis L.) seed in a fixed bed tubular reactor. Chem Eng Trans 37: 127–132
52. Bishop CM (1995) Neural networks for pattern recognition. Oxford University Press, New York
53. Yan C, Li G, Xue P, Wei Q, Li Q (2010) Competitive effect of Cu (II) and Zn (II) on the biosorption of lead (II) by Myriophyllum spicatum. J Hazard Mater 179(1):721–728
54. Gupta N, Kushwaha AK, Chattopadhyaya MC (2012) Adsorptive removal of Pb^{2+}, Co^{2+} and Ni^{2+} by hydroxyapatite/chitosan composite from aqueous solution. J Taiwan Inst Chem Eng 43(1):125–131
55. Prasad RK, Srivastava SN (2009) Sorption of distillery spent wash onto fly ash: Kinetics, mechanism, process design and factorial design. J Hazard Mater 161(2):1313–1322
56. Mohammadi AA, Zarei A, Alidadi H, Afsharnia M, Shams M (2018) Two-dimensional zeolitic imidazolate framework-8 for efficient removal of phosphate from water, process modeling, optimization, kinetic, and isotherm studies. Desalin Water Treat 129:244–254
57. Foo KY, Hameed BH (2010) Insights into the modeling of adsorption isotherm systems. Chem Eng J 156(1):2–10
58. Dehghani MH, Zarei A, Mesdaghinia A, Nabizadeh R, Alimohammadi M, Afsharnia M, McKay G (2018) Production and application of a treated bentonite–chitosan composite for the efficient removal of humic acid from aqueous solution. Chem Eng Res Des 140:102–115
59. Al-Ghouti MA, Da'ana DA (2020) Guidelines for the use and interpretation of adsorption isotherm models: a review. J Hazard Mater 122383
60. Crini G, Peindy HN, Gimbert F, Robert C (2007) Removal of CI Basic Green 4 (Malachite Green) from aqueous solutions by adsorption using cyclodextrin-based adsorbent: Kinetic and equilibrium studies. Sep Purif Technol 53(1):97–110
61. Robati D (2013) Pseudo-second-order kinetic equations for modeling adsorption systems for removal of lead ions using multi-walled carbon nanotube. J Nanostructure Chem 3(55):1–6
62. Ganguly P, Sarkhel R, Das P (2020) Synthesis of pyrolyzed biochar and its application for dye removal: batch, kinetic and Isotherm with linear and non-linear mathematical analysis. Surf Interfaces 20: 100616
63. Reczeka L, Michela MM, Domozychb A, Siwieca T, Tytkowskaa M, Świątkowskic A (2020) Effect of lead (II) presence on sorption of 4-chlorophenol on synthetic activated carbon. Desalin Water Treat 186:247–257
64. Jasper EE, Ajibola VO, Onwuka JC (2020) Nonlinear regression analysis of the sorption of crystal violet and methylene blue from aqueous solutions onto an agro-waste derived activated carbon. Appl Water Sci 10(6):1–11
65. Hossain MD, Ngo H, Guo W (2013) Introductory of Microsoft Excel SOLVER function-spreadsheet method for isotherm and kinetics modelling of metals biosorption in water and wastewater. J Water Sustain 3(4):223–237
66. Ngakou CS, Anagho GS, Ngomo HM (2019) Non-linear regression analysis for the adsorption kinetics and equilibrium isotherm of phenacetin onto activated carbons. Curr J Appl Sci Technol 1-18

67. Haq S, Rehman W, Waseem M, Rehman MU, Shah KH (2019).Modeling, thermodynamic study and sorption mechanism of cadmium ions onto isopropyl alcohol mediated tin dioxide nanoparticles. J Inorg Organomet Polym Mater 1-9
68. Brasil JL, Ev RR, Milcharek CD, Martins LC, Pavan FA, Dos Santos AA, Dias SLP, Dupont J, Noreña CPZ, Lima EC (2006) Statistical design of experiments as a tool for optimizing the batch conditions to Cr (VI) biosorption on Araucaria angustifolia wastes. J Hazard Mater 133(1):143–153
69. Pavan FA, Gushikem Y, Mazzocato AC, Dias SLP, Lima EC (2007) Statistical design of experiments as a tool for optimizing the batch conditions to methylene blue biosorption on yellow passion fruit and mandarin peels. Dyes Pigments 72(2):256–266
70. Saadat S, Karimi-Jashni A (2011) Optimization of Pb (II) adsorption onto modified walnut shells using factorial design and simplex methodologies. Chem Eng J 173(3):743–749
71. Ghaedi AM, Vafaei A (2017) Applications of artificial neural networks for adsorption removal of dyes from aqueous solution: a review. Adv Colloid Interfac 245:20–39
72. Hecht-Nielsen R (1992) Theory of the backpropagation neural network. In Neural networks for perception. Academic Press, pp 65-93
73. Orhan U, Hekim M, Ozer M (2011) EEG signals classification using the K-means clustering and a multilayer perceptron neural network model. Expert Syst Appl 38(10):13475–13481
74. Hagan MT, Demuth HB, Beale MH (1996) Neural network design. PWS Publishing, Boston, MA
75. Alsultanny YA, Aqel MM (2003) Pattern recognition using multilayer neural-genetic algorithm. Neurocomputing 51:237–247
76. Das L, Das P, Bhowal A, Bhattachariee C (2020) Synthesis of hybrid hydrogel nano-polymer composite using graphene oxide, chitosan and PVA and its application in waste water treatment. Environ Technol Innov 18:100664
77. Silva TS, de Freitas SM, da Silva Teófilo TM, dos Santos MS, Porto MAF, Souza CMM, dos Santos JB, Silva DV (2019) Use of neural networks to estimate the sorption and desorption coefficients of herbicides: a case study of diuron, hexazinone, and sulfometuron-methyl in Brazil. Chemosphere 236:124333
78. Dutta S, Parsons SA, Bhattacharjee C, Bandhyopadhyay S, Datta S (2010) Development of an artificial neural network model for adsorption and photocatalysis of reactive dye on TiO_2 surface. Expert Syst Appl 37(12):8634–8638
79. Fletcher D, Goss E (1993) Applications forecasting with neural networks: an application using bankruptcy data. Inf Manag 24: 159–167
80. Zhong ZY, Yang Q, Li XM, Luo K, Liu Y, Zeng GM (2012) Preparation of peanut hull-based activated carbon by microwave-induced phosphoric acid activation and its application in Remazol Brilliant Blue R adsorption. Ind Crop Prod 37(1):178–185
81. Cardoso NF, Pinto RB, Lima EC, Calvete T, Amavisca CV, Royer B, Cunha ML, Fernandes THM, Pinto IS (2011) Removal of remazol black B textile dye from aqueous solution by adsorption. Desalination 269:92–103
82. Saxena M, Sharma N, Saxena R (2020) Highly efficient and rapid removal of a toxic dye: adsorption kinetics, isotherm, and mechanism studies on functionalized multiwalled carbon nanotubes. Surf Interfaces 21:100639
83. Rizk HE, Attallah MF, Ali AMI (2017) Investigations on sorption performance of some radionuclides, heavy metals and lanthanides using mesoporous adsorbent material. J Radioanal Nucl Chem 314(3):2475–2487
84. Kamga FT (2019) Modeling adsorption mechanism of paraquat onto Ayous (Triplochiton scleroxylon) wood sawdust. Appl Water Sci 9(1):1
85. Wu P, He Y, Lu S, Wang S, Yi J, He Y, Zhang J, Xiang S, Ding P, Kai T, Pan H (2020) A regenerable ion-imprinted magnetic biocomposite for selective adsorption and detection of Pb2+ in aqueous solution. J Hazard Mater 124410
86. Kavak D (2009) Removal of boron from aqueous solutions by batch adsorption on calcined alunite using experimental design. J Hazard Mater 163:308–314
87. Anderson MJ (2001) A new method for non-parametric multivariate analysis of variance. Austral Ecol 26(1):32–46
88. Darvishmotevalli M, Zare A, Moradnia M, Noorisepehr M, Mohammadi H (2019) Optimization of saline wastewater treatment using electrochemical oxidation process: Prediction by RSM method. MethodsX 6:1101–1113
89. Safa Y, Bhatti HN (2011) Biosorption of direct red-31 and direct orange-26 dyes by rice husk: application of factorial design analysis. Chem Eng Res Des 89:2566–2574
90. Gottipati R, Mishra S (2010) Process optimization of adsorption of Cr (VI) on activated carbons prepared from plant precursors by a two-level full factorial design. Chem Eng J 160(1):99–107
91. Rathinam A, Rao JR, Nair BU (2011) Adsorption of phenol onto activated carbon from seaweed: determination of the optimal experimental parameters using factorial design. J Taiwan Inst Chem Eng 42:952–956
92. Özbay N, Yargıç AŞ, Yarbay-Şahin RZ, Önal E (2013) Full factorial experimental design analysis of reactive dye removal by carbon adsorption. J Chemother 2013:1–13
93. Bingol D, Tekin N, Alkan M (2010) Brilliant Yellow dye adsorption onto sepiolite using a full factorial design. Appl Clay Sci 50(3): 315–321
94. Kaouah F, Boumaza S, Berrama T, Trari M, Bendjama Z (2013) Preparation and characterization of activated carbon from wild olive cores (oleaster) by H_3PO_4 for the removal of Basic Red 46. J Clean Prod 54:296–306
95. McCulloch WS, Pitts W (1943) A logical calculus of the ideas immanent in nervous activity. Bull Math Biol 5(4):115–133